Soil-air phase characteristics: Response to texture, density, and land use in Greenland and Denmark.

Pesch, Charles; Jensen, Peter Weber; de Jonge, Lis Wollesen; Greve, Mogens Humlekrog; Nørgaard, Trine; Møldrup, Per

Published in:
Soil Science Society of America Journal

DOI (link to publication from Publisher):
10.1002/saj2.20284

Publication date:
2021

Document Version
Accepted author manuscript, peer reviewed version

Core ideas

- We analyzed air-phase characteristics of Danish and Greenlandic soils.
- The air phase revealed within-field variability not captured by the water phase.
- Structure-related fingerprints differentiated between land use (LU) and texture.
- The across-field air-phase characteristic was accurately predicted by LU and texture.
- The air-filled porosity was precisely estimated by a modeled response surface.

Abbreviations

Abbreviation	Explanation
OC	organic carbon content
fines	gravimetric fraction of particles $< 20\,\mu m$
fS	gravimetric fraction of particles $[50 - 200]\,\mu m$
TUI	texture uniformity index, ratio fS/fines
LU	categorical land-use variable
WRC	soil-water retention curve
SAC	soil-air characteristic curve
MRS	modeled response surface
ρ_b	dry bulk density
Φ	total porosity
ε	air-filled porosity
ψ	soil-water matric potential
pF	decadal logarithm of $\lvert\psi\rvert$
D_p/D_o	relative diffusivity
k_a	air permeability
X	connectivity-tortuosity index
Ω	soil-structure index

Soil-air phase characteristics: Response to texture, density, and land use in Greenland and Denmark[†].

Charles Pesch[1], Peter L. Weber[2], Lis W. de Jonge[2], Mogens H. Greve[2], Trine Norgaard[2], and Per Moldrup[1]

[1]Dep. of the Built Environment, Faculty of Engineering and Science, Aalborg Univ., Thomas Manns Vej 23, DK-9220 Aalborg, Denmark
[2]Dep. of Agroecology, Faculty of Techincal Sciences, Aarhus Univ., Blichers Allé 20, P.O. Box 50, DK-8830 Tjele, Denmark

August 30, 2021

Abstract

Soil aeration is a key parameter for sustainable and productive agriculture. The intensification of agricultural activity in Greenland involves land use and land-use change, affecting the soil-air phase. The combined effects of natural compaction (bulk density, ρ_b), texture (TUI), and land use (LU) on the soil-air phase of subarctic soils are not well known. This study aims to identify and compare the main drivers for air-filled porosity (ε) and soil-structure changes within and across sites in Greenland and Denmark. We analyzed comprehensive data sets of ε, relative gas diffusivity (D_p/D_o), and air-permeability (k_a) measured on intact soil samples from South-Greenland (pasture) and Denmark (cultivated, urban, and forest). The mechanical robustness of the air phase was evaluated by linear models of ε as a function of ρ_b (H-model). The ratio of k_a to D_p/D_o served as a soil-structure index (Ω; the latter significantly correlated to TUI. The Greenlandic pasture soils did not show signs of well-developed soil structure (low Ω-values), while low H-values suggested the soils were mechanically robust compared to similar-textured cultivated soils. The soil-air characteristic curve (ε versus pF) was parameterized, and the moisture control parameter was accurately predicted by TUI and LU ($R^2 = .95$). Overall, the ρ_b was found to control the air-phase functions within a field. However, considering changes in ε-levels across different fields, texture, land use, and other environmental factors became statistically more relevant than ρ_b. A modeled response surface for changes in ε with soil conditions may, in perspective, be useful for better-predicting gas transport in soil, both within and across fields.

Keywords: Soil-air phase, air-filled porosity, compaction, soil structure, modeled response surface (MRS)

[†] Published as: Pesch, C., Weber, P. L., de Jonge, L. W., Greve, M. H., Norgaard, T., Moldrup, P., 2021. Soil–air phase characteristics: Response to texture, density, and land use in Greenland and Denmark. Soil Science Society of America Journal, 1–21 https://doi.org/10.1002/saj2.20284

1 Introduction

For many decades, soil aeration has been extensively studied in relation to plant and root growth (Cannon and Free, 1917; Williamson, 1964; Stepniewski et al., 2011) or for monitoring and remediation of sub-surface contamination (Poulsen et al., 1998, 1999). The climatic impacts due to the emissions of radiatively-active gases from the sub-surface to the atmosphere have been widely acknowledged (Gregorich et al., 2005; Smith et al., 2012; Ball, 2013), and methods to estimate, simulate, and reduce these emissions are continuously being refined (e.g., Johnson et al., 2007; Deepagoda et al., 2011b; Li et al., 2017).

The soil's structure plays a paramount role in soil aeration and gas-exchange processes, and a multitude of factors controls it. The underlying controlling and regulating entities are the geological background, which governs the availability of the basic mineral material, the climatic conditions, which control weathering, biological and anthropogenic processes (Kerr, 1952; Reynolds, 1971; Folkoff and Meentemeyer, 1987), and time (Uteau et al., 2013; Egli et al., 2018).

A major component of soil-structure development is the soil's potential to form aggregates. The formation and stability of soil aggregates are to a large extent controlled by texture (Wagner et al., 2007), microbial activity, and soil-organic matter quality (Annabi et al., 2011), whereby, in particular the latter two, are substantially influenced by land use and land management (Ball et al., 1997; Bottinelli et al., 2017).

To study the effect of cold climatic conditions and time on the development of agriculturally exploited soils, the western part of South-Greenland is ideal. With an annual average temperature of 1.2 °C and a cumulative precipitation of 612.9 mm (Narsarsuaq, 1961-2018, Cappelen, 2019), the area is situated at the climatic limits at which agricultural production is feasible. In some areas, the rather recent retraction of glaciers (Carlson et al., 2014) formed relatively young soils compared to soils found in temperate regions. Agricultural activity in Greenland mainly consists of sheep-husbandry. The necessary winter-fodder production is carried out on low-lying, more or less fertile, generally sandy lands, whereas the areas at higher elevations are used as summer-pastures. Climate change might alter the accustomed agricultural methods towards a more labor-intensive practice and entail a change in land use and land management, which, in turn, eventually will change the current soil-ecological equilibrium.

Changes in soil structure can be characterized by changes in the pore-size distribution of the porous soil-matrix. The pore size distribution may be altered by compaction due to climate, land-cover, and agricultural activity by, e.g., cattle and field-traffic. Changes in bulk density (ρ_b) are directly reflected in the pore-size distribution. Compaction obviously results in an overall reduction of the total porosity (Φ), but more importantly, it results in a shift in the pore-size distribution with a reduction of the macro-porosity ($D_\phi > 30\,\mu m$, pore diameter D_ϕ) and an increase in micro-porosity ($D_\phi < 6\,\mu m$) (Lipiec et al., 2012). Dörner et al. (2016) and Dlapa et al. (2020) showed that land use and land-use change had significant negative effects on the water-retention and air-phase characteristics in terms of soil-aeration processes.

Several studies have shown that soil structure and air-phase tortuosity could be quantified and qualified by gas-flow measurements (e.g., air permeability, relative gas diffusivity, and combinations of both) through the porous medium. Deepagoda et al. (2012) revealed that changes in the connectivity-tortuosity parameter X (Buckingham, 1904; Currie, 1960a) along a moisture gradient could be used to differentiate between

inter- and intra-aggregate pore space. Moldrup et al. (2003a) used the equivalent pore diameter to characterize the pore connectivity, and thus the presence of soil structure, along a soil-water potential gradient of differently textured soils exhibiting different land use and management. A similar approach was used by Kawamoto et al. (2006), who related air permeability to relative diffusivity measurements, where the latter was estimated by the relation suggested by Moldrup et al. (2000b) and solely relying on ε measurements at a fixed soil-water potential.
More complex prediction models incorporate soil-type dependent information (Moldrup et al., 2000b), generally in the form of a parameter describing the water retention characteristic. Moldrup et al. (1996) used the well known Campbell (1974) water retention model to predict gas diffusivity; Moldrup et al. (1999) extended the approach into the Buckingham-Burdine-Campbell gas diffusivity model. Similar power law models exist for modeling the air permeability of variably saturated soils (Kawamoto et al., 2006; Assouline et al., 2016). The interested reader may additionally refer to the comprehensive work on air permeability models carried out by Yang et al. (in press, 2021)
The above-mentioned studies revealed that the gaseous exchange processes within the soil and between soil and atmosphere heavily rely on the pore-space available for gas transport, i.e., the air space not filled by water. However, many of the available prediction models for gas transport parameters incorporate some form of water-retention parameters, which do not represent the air-filled, but the water-filled porosity, and thus not taking into account the potentially significant differences in the variability of the air-filled porosity compared to water-filled porosity.
Instead of parameters derived from the soil-water retention curve, the use of derived parameters from a soil-air characteristic curve in soil-air function predictions would be more straightforward and might eventually reduce the not-explained variability of those models.

1.1 Objectives

The objective of this study is to understand how soil texture (texture uniformity), compaction (dry bulk density), and land use (land use type) combined affect key soil-gas phase parameters across moisture conditions (at different levels of soil-water matric potential, as quantified by pF). Specifically, we aim to

(i) provide a dual-fingerprint for soil structure that in perspective may allow us to better predict the key soil-gas transport parameters (diffusivity and permeability)

(ii) understand and quantify (by a modeled response surface) combined effects of dry bulk density and pF on air-filled porosity at given indices for land use and texture.

First, we illustrate that the water retention curve, the derived soil-air characteristic curve, and gas transport parameter curves (gas diffusivity and air permeability) vary considerably across and within fields with very different texture and land use. Second, we combine soil-gas phase parameters to make a dual-fingerprint of soil-gas phase behavior related to soil moisture level (pF). Third and based on these analyses, we develop and verify a modeled response surface for the soil air-filled porosity by combining two linear models for changes in air-filled porosity with dry bulk density and with pF, and with the slopes in the two models related to texture or land-use indices, or both.

We base this three-part analyses on data from 966 intact soil core samples from 14 differently textured South Greenlandic (pasture) and Danish (cultivated, urban, and forest) soils, hereby representing a wide range of soil texture, compaction, and land use

2 Material and Methods

2.1 Soils and soil sampling

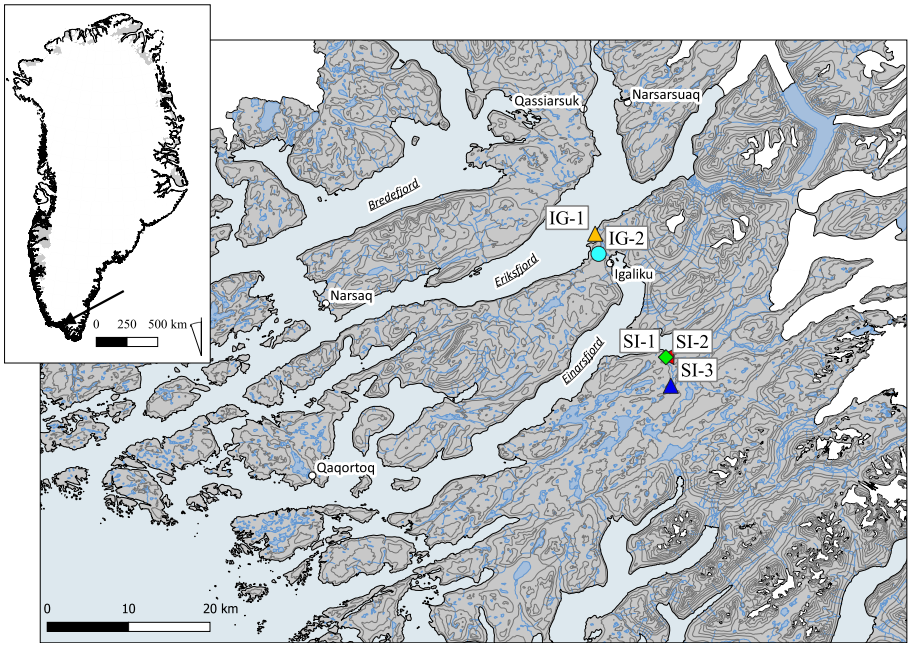

FIGURE 1: The five sampling sites in South Greenland.

In total, data from 966 individual, intact soil core samples (6.05 cm in diameter, 3.48 cm height, resulting in a volume of 100 cm^3) was collected and evaluated. The soil cores originated from 14 different sites located across south-west Greenland and Denmark and included four different land uses (cultivated, pasture, urban, and forest). Table 1 gives an overview of the sampling sites and soils used in this study. The Greenlandic data-set consisted of five perennial pasture soils, and the sampling locations are shown in Fig.1. The Danish data-set comprised five conventionally cultivated, two urban, and one forest soil. For the localization of the Danish soils, the reader may refer to the geographical coordinates given in Table 1.
The Greenlandic pasture and Danish cultivated soils were sampled in rectangular grids (15 m × 15 m, except South Igaliku 2, which was sampled in a 7.5 m × 7.5 m grid). The grid-sampled soil-cores were extracted from the soil's upper horizon from a depth varying between 5 and 15cm.
The Danish cultivated soils were sampled throughout the peninsula of Jutland, and, in total, 551 individual soil cores were included in this study (226 individual sampling points, varying number of replicates per point). The soil textures ranged from coarse sand (Jyndevad) to silty clay loam (Voldbjerg), covering the most abundant soil-textural classes of agriculturally exploited soils in Denmark. The sampling of the Danish cultivated soils was carried out between 2010 and 2014, and none of the fields were cultivated (plowed) approximately one year prior to the sampling. The cultivated soils were previously published in other studies, and a detailed description of the different sites' geological

TABLE 1: Geographical information of the sites the samples were collected from and the soil classification according to Soil Survey Staff (1999).

Site	Country	Coordinates	Soil classification†	Reference
Jyndevad*	Denmark	N54°53′37″ E9°7′12″	Typic Haplorthods	Masís-Meléndez et al. (2014)
Tylstrup*		N57°10′47″ E9°57′24″	Humic Psammentic Dystrudept	Karup et al. (2016)
Estrup*		N55°29′10″ E9°4′9″	Abrupt/Aqua Argiudoll, Frangiaquic Glossudalf	Paradelo et al. (2015)
Silstrup*		N56°55′56″ E8°38′44″	Alfic Argiudoll, Typic Hapludoll	Norgaard et al. (2013)
Voldbjerg		N56°18′71″ E8°54′87″	Aquic Palehumults	Karup et al. (2016)
South Igaliku 1 & 2	Greenland	N60°53′29″ W45°16′28″	Lithic Dystrocryept	Weber et al. (2020); Pesch et al. (2020)
South Igaliku 3		N60°51′39″ W45°16′26″	Psammentic Dystrocryept	
Igaliku 1		N61°1′9″ W45°27′39″	Typic Dystrocryept	Weber et al. (2020)
Igaliku 2		N60°59′51″ W45°26′55″	Typic Dystrocryept	
Skellingsted	Denmark	N55°35′25″ E11°27′44″	Filled Anthropic soil	Poulsen et al. (2001)
Hjørring		N57°27′34″ E10°0′1″	Mixed Anthropic soil	Moldrup et al. (2000b)
Poulstrup		N57°21′30″ E10°0′38″	Spodosol (not further specified)	Kruse et al. (1996); Moldrup et al. (1996)

* detailed monitoring site description can also be found in Lindhardt et al. (2001)

† If more than one classification per site is given, more than one soil profile was evaluated and different results were obtained.

background and land management can be found in the relevant studies (Hermansen et al., 2017; Karup et al., 2016; Paradelo et al., 2015; Katuwal et al., 2015; Masís-Meléndez et al., 2014; Norgaard et al., 2013). Additionally, Jyndevad, Tylstrup, Estrup and Silstrup are part of the Danish Pesticide Leaching Assessment Program (PLAP), and detailed information about the specific sites can be found in Lindhardt et al. (2001). The Greenlandic sites are described in Weber et al. (2020) and Pesch et al. (2020). In total, 396 individual soil core samples from five pasture fields from south-west Greenland were included in this study (132 individual sampling points, three replicates per point). The sampling was carried out in 2015 (South Igaliku 1, 2, and 3) and 2017 (Igaliku 1 and 2); the soil cover during sampling consisted of perennial grass, and besides field Igaliku-1, no cultivation or tillage was carried out at least three years prior to the sampling. The grass cover is occasionally resown, especially if frost and water damage becomes prevalent. Tillage consists of disc harrowing ($5 - 10$ cm depth); plowing is generally avoided due to the high wind erosion hazard of the sandy to sandy-loamy soils, especially in combination with the frequent, intense katabatic winds in the area. To our knowledge, South Igaliku 1 and 2 have not been subjected to tillage during the last 20 years and are used as pastures for grazing sheep. The fields Igaliku-1, Igaliku-2, and South Igaliku-3, are mainly used for winter fodder production.

In order to broaden the range of covered land uses within this study, three additional sites exhibiting two different land uses were included.

The soils categorized as urban soils were collected from a soil profile (Hjørring, North Jutland, Denmark) and from a sub-soil transect (Skellingsted, Zealand, Denmark). The samples from Hjørring were collected during the drilling of a monitoring-well on a former manufactured gas plant site. Sub-samples of the initial drilling core samples (4 to 5 and 6 to 7 m soil depth) were taken at equal distance (0.4 m) throughout the soil profile. The samples from Skellingsted were collected along a transect on an abandoned landfill site from a depth of 70 cm, consisting of an artificially compacted, industrial sand cover-layer.

The forest soil samples (Poulstrup, North Jutland, Denmark) were collected from four different depth-intervals (0-5, 5-10, 10-15, and 15-20 cm soil depth) below a deciduous forest. The forest soil data-set was subdivided into two sub-sets due to the very distinct soil properties of the top and sub-soil; Poulstrup top-soil comprised the two depth-intervals down to 10 cm included, Poulstrup sub-soil consists of the remaining 10-15 cm and 15-20 cm depth-intervals.

Along with the intact soil core samples, bulk soil from the same depth was collected at each sampling point for texture analysis in the laboratory. For the data analysis, the

intact soil-core replicates per sampling point were treated as individual samples.

2.2 Laboratory methods

2.2.1 Basic soil characteristics

The bulk soil samples collected at each sampling point were air-dried and pre-sieved ($< 2\,\mathrm{mm}$) prior to texture analysis and organic carbon content (OC, in $\mathrm{g\,g^{-1}}$) determination. The texture was determined using a combination of wet sieving and the hydrometer or pipette method, according to Gee and Or (2002). Total carbon was measured on ball-milled samples by dry combustion in combination with an infrared CO_2 detector. All the soils were free of carbonates, and the measured total carbon was thus set equal to organic carbon. The average particle density, ρ_s [$\mathrm{g\,cm^{-3}}$], was estimated from organic matter and clay contents, according to Schjønning et al. (2017).

2.2.2 Soil-water retention characteristics

In order to determine the water-retention characteristics, the intact soil core samples were saturated from below on a tension table and subsequently drained to all or to a selection of the following matric-potentials:
$\psi\,[\mathrm{cm\,H_2O}] \in \{-10, -30, -50, -100, -300, -500, -1000\}$. The drainage procedure followed the procedure given in Dane and Hopmans (2002). Based on the magnitude of the intended negative soil-water potentials (ψ), different apparatus and procedures were used: hanging water column for $-100 \leq \psi\,[\mathrm{cm\,H_2O}] \leq -10$, suction plate for $-500 \leq \psi\,[\mathrm{cm\,H_2O}] < -100$, and pressure plates for $\psi\,[\mathrm{cm\,H_2O}] < -500$.
After equilibration of the soil sample with the applied negative potential, the mass loss was determined on a laboratory scale and set equal to the gravimetric soil-water release during the drainage step. The volumetric water content, θ [$\mathrm{cm^3\,cm^{-3}}$] was obtained by multiplication of the gravimetric water content with the dry bulk density. The air-filled porosity, ε [$\mathrm{cm^3\,cm^{-3}}$] was obtained by $\varepsilon = \Phi - \theta$, with Φ [$\mathrm{cm^3\,cm^{-3}}$] being the total porosity.

2.2.3 Soil-air phase functions

At each drainage step, the air permeability and the relative gas diffusivity were determined. The air permeability (k_a in $\mu\mathrm{m^2}$) of the forest and urban soils were measured by the steady-state method, according to the procedure and device described in Iversen et al. (2001) and Ball and Schjønning (2002); the k_a of the cultivated and pasture soils were measured using the device described in Schjønning and Koppelgaard (2017), following the guidelines given in Ball and Schjønning (2002). The gaseous phase's diffusive movement through the unsaturated soil matrix was assessed by the non-steady, single chamber method suggested by Taylor (1950) and further developed by Schjønning (1985). Oxygen was used as the diffusing agent, and the apparent diffusion coefficient of the soil, D_p [$\mathrm{cm^2\,s^{-1}}$], was calculated, according to Taylor (1950). The relative diffusivity, D_p/D_o (dimensionless), was then obtained by dividing D_p by the diffusion coefficient of oxygen in free air, $D_o = 0.205\,\mathrm{cm^2\,s^{-1}}$ at 20 °C (Schjønning et al., 2013). A comprehensive description of the different aspects and procedures of the measurement can be found in Rolston and Moldrup (2002).
After the final drainage step, the dry bulk density of the intact soil-core samples, ρ_b [$\mathrm{g\,cm^{-3}}$], was measured after oven-drying for 24 to 48 h at 105 °C.

For the sake of simplicity, the soil-water potential is given as pF = $\log(-\psi)$, ψ in cm H_2O (Schofield, 1935).
Additionally, two notations need to be defined: the notation *across-field* variation was defined as the variation of the field-averaged parameter in question between at least two fields, whereas the *within-field* variation covered variations inherent to one specific field. The field-average value of a soil property was calculated as the arithmetic mean of all the individual measurements available for the relevant property for a given field; its variation was assessed by the standard deviation and illustrated by error-bars in the figures.

2.3 Models

2.3.1 H-model

The within-field dependence of the air-filled porosity (ε) on the bulk density (ρ_b) for each soil-water potential level (pF) was assessed by fitting the linear function given in Eq. (1) to the measured ε at each available drainage level and ρ_b. The model will hereafter be referred to as the H-model:

$$\varepsilon = -H \cdot \rho_b + C\,, \tag{1}$$

where H and C represent the slope and the intercept, respectively, we thus obtained a maximum of seven individual regression lines per field (maximum of seven drainage steps), where H describes the sensitivity of the air-filled porosity to changes in natural compaction (ρ_b).

TABLE 2: H-indices for a theoretical pure sand from assumed ρ_b and θ_g-ranges, determined by using Eq. (1). ρ_s was fixed to 2.65 g cm^{-}3. θ_g and θ_v denote the gravimetric and volumetric water contents, respectively.

θ_g	ρ_b	Φ	θ_v	ε	H
[g g^{-1}]	[g cm^{-3}]	[cm^3 cm^{-3}]			[–]
†0.05	1.4	0.47	0.07	0.40	0.43
	1.6	0.40	0.08	0.32	
‡0.20	1.4	0.47	0.28	0.19	0.58
	1.6	0.40	0.32	0.08	

†dry soil, high pF; ‡wet soil, low pF

The H-range of a theoretical pure sand will be used to evaluate and contrast the H-values obtained on intact soil cores. The expected H-range for a pure sand at low and high moisture conditions can be estimated by assuming reasonable ρ_b- and a θ_g-ranges for such material. We used the soil conditions and properties given in Table 2. The H-values of the resulting theoretical pairs of measurements (ρ_b, ε) at the two moisture levels were then determined by fitting the H-model as given in Eq. (1).

2.3.2 Soil-air characteristic model

Similar to the Gregson et al. (1987) semi-logarithmic model for soil-water retention, the variation of ε with varying moisture conditions can be approximated in the $\log(-\psi) - \varepsilon$ domain.

The resulting log-linear (semi-logarithmic) soil air characteristic curve (SL-SAC) exhibits two parameters: the reference air-filled porosity, ε_{ref}, which is the ε at the reference soil-water potential, pF_{ref}, and the soil-air characteristic parameter, A. The A-model is fully defined if ε_{ref} (location parameter) and A (shape parameter) are known:

$$\varepsilon = \varepsilon_{ref} - A \cdot \left(\mathrm{pF}_{ref} - \mathrm{pF}\right) . \tag{2}$$

The introduction of a reference point other than the phase content at saturation (which would be $\varepsilon(\psi = 0) = 0$ in this case) is not a new concept, as it was already applied with success by other authors (Pittaki-Chrysodonta et al., 2018).

2.3.3 Modeled response surface (MRS)

The A- and H-model were eventually combined to express the air-filled porosity as a function of ρ_b and pF only. Substituting ε_{ref} in Eq. (2) by the relation given in Eq. (1) generates the multi-variable function given in Eq. (3), and its output will be referred to as modeled response surface (MRS):

$$\varepsilon = \left[- H \cdot \rho_b + C\right] - A \cdot \left(\mathrm{pF}_{ref} - \mathrm{pF}\right) . \tag{3}$$

The main model parameters A and H need to be known beforehand, and we will show over the course of this study that it is possible to predict both very accurately from basic soil properties.

2.3.4 Gas-diffusion model

The diffusive gas movement in the soil-air phase, which originates from concentration gradients within the porous matrix, is the principal gaseous exchange process in the soil (Rolston and Moldrup, 2002). It can be evaluated by the relative gas diffusion coefficient or gas diffusivity, D_p/D_o, with D_p and D_o being the gas diffusion coefficient in the soil and in free air, respectively. Many studies (Buckingham, 1904; Currie, 1960b, 1961; Millington and Quirk, 1961; Moldrup et al., 2003b, 2004; Thorbjørn et al., 2008, etc.) have assumed or ascertained that D_p/D_o is governed to a large extend by texture, soil-air content (ε) and total porosity (Φ). Buckingham (1904) suggested that D_p/D_o follows a power function of ε:

$$D_p/D_o = \varepsilon^X , \tag{4}$$

where X was later referred to as the connectivity-tortuosity parameter (Currie, 1960b, 1961).

2.3.5 Ω-model

The contrasting behavior of advective and diffusive flows to the pore geometry (Millington and Quirk, 1964; Ball, 1981) enables a direct assessment of soil structure (Kawamoto et al., 2006; Eden et al., 2011; Arthur et al., 2012). Kawamoto et al. (2006) derived a prediction model for k_a from D_p/D_o, and a simplified version of the model is given in Eq. (5):

$$k_a = \Omega \cdot \varepsilon^X , \text{ with } \quad \varepsilon^X = (D_p/D_o) , \tag{5}$$

where ε and X are the air-filled porosity and the connectivity-tortuosity parameter, respectively, and Ω is a soil-structure index. Kawamoto et al. (2006) found the best agreement between k_a and D_p/D_o for $\Omega = 700$, based on 25 differently textured soil layers. For soils exhibiting $\Omega > 700$, the advective flow exceeds the diffusive flow, and a more pronounced soil-structure can be expected (larger connected macro-porosity).

2.3.6 Texture uniformity index

Soil texture was characterized by the field-average ratios of the gravimetric contents of fine sand (fS, $50 < D_e < 200\,\mu m$, D_e denotes the equivalent particle diameter) and fine particles (fines, $D_e < 20\,\mu m$), referred to as soil texture uniformity index (TUI, dimensionless). D_e and fines represent the equivalent particle diameter and the sum of the clay and fine silt fractions, respectively:

$$\mathrm{TUI} = \mathrm{fS}/\mathrm{fines}\,. \tag{6}$$

The fine fraction of the mineral soil ($D_e < 20\,\mu m$) largely controls soil-aggregate formation, primarily by self-aggregation and complexation with available soil-organic matter (Chesters et al., 1957; Schjønning et al., 1999; Dexter et al., 2008). Since soils considered in this study generally exhibited high ratios of organic matter to fine particles, the differences in the composition of the fine-textured mineral phase ($D_e < 200\,\mu m$) become the main driver for aggregation and structure formation; the TUI describes these differences in a simple way. Additionally, relations between coarse and fine particles were already found to be useful for successfully predicting hydraulic soil properties, which are undoubtedly closely related to soil structure (Arya and Paris, 1981; Nielsen et al., 2018).

2.4 Statistical Analysis

The Pearson correlation coefficient r assessed the linear correlation between two continuous variables. The significance level of any fitted or estimated parameter was depicted by stars appended as an exponent to the parameter in question, according to the levels of significance: $(^{***})$ if $p < .001$, $(^{**})$ if $.01 < p \leq .001$, $(^{*})$ if $.01 \leq p < 0.05$ and for no significance, $(^{ns})$ if $p \geq .05$.
The linear relations between the investigated properties and parameters were evaluated by simple or multiple ordinary least-squares regressions. The goodness of fit and the model performance were judged by the ordinary and adjusted coefficient of determination, R^2 (simple) and R^2_{adj} (multiple), respectively, the root-mean-square error, RMSE, and the Akaike information criterion, AIC (Sakamoto et al., 1986), specifically by the AICc, accounting for small sample sizes according to Sugiura (1978).
For determining the confidence and prediction intervals of the H-model's regression coefficients (Eq (1)), we deployed a non-parametric bootstrapped regression scheme. The base for the computation of the required bootstrapped regression coefficients and statistics was the random resampling of pairs of observations with replacement (Efron, 1979, 1983; Stine, 1985). The resampling was based on 75% of the total number of available observations, and the resampling was repeated 1000 times. The confidence and prediction intervals were computed as the 5.0% and 95.0% percentiles of the relevant bootstrapped parameter, leading to 90.0% ($\alpha = .10$) confidence and prediction intervals. The goodness of fit (only R^2) and the overall significance of the regression (p-value of the F-statistic) were given as mean values of the bootstrapped results.

The statistical analysis was entirely carried out in MATLAB and Statistics Toolbox (2018).

3 Results and Discussion

3.1 Combined effects of texture, density, and land use on gas-phase behavior

TABLE 3: Summary table of the basic soil properties and the number of individual undisturbed soil core samples (number of sampling points per site in parentheses); soil type and particle size distribution; texture uniformity index, TUI (dimensionless); the organic carbon content (OC); the dry bulk density (ρ_b). All displayed figures are mean values, and the figures in parentheses represent the standard deviation. ND stands for not determined.

Site	Samples	Soil type	Clay ($< 2\,\mu m$)		Silt ($2 - 50\,\mu m$)				Sand ($50 - 2000\,\mu m$)				TUI		OC		ρ_b	
	(& Points)	USDA			fine ($< 20\,\mu m$)		coarse [$g\,100\,g^{-1}$]		fine ($< 200\,\mu m$)		coarse		[–]		[$g\,100\,g^{-1}$]		[$g\,cm^{-3}$]	
Jyndevad	88 (88)	S	4.2	(0.4)	3.7	(0.4)	1.0	(0.0)	23.4	(0.9)	64.4	(1.2)	3.0	(0.2)	1.8	(0.2)	1.38	(0.04)
Tylstrup	72 (36)	lS-sL	3.8	(0.2)	7.0	(0.9)	12.4	(1.5)	63.7	(1.8)	9.9	(1.3)	6.0	(0.7)	1.8	(0.1)	1.34	(0.05)
Estrup	135 (45)	sL-lS	10.9	(2.1)	12.4	(2.4)	12.5	(2.6)	22.5	(1.2)	37.0	(5.6)	1.0	(0.2)	2.6	(0.7)	1.36	(0.10)
Silstrup	180 (60)	sL-L	15.8	(1.3)	16.5	(1.0)	13.6	(1.3)	28.9	(1.4)	21.8	(1.8)	0.9	(0.1)	1.9	(0.1)	1.43	(0.07)
Voldbjerg	36 (9)	cL-ucL	31.5	(1.4)	22.9	(1.1)	18.8	(3.6)	13.0	(3.6)	9.3	(2.2)	0.3	(0.1)	2.6	(0.4)	1.26	(0.06)
South Igaliku-2	54 (18)	lS-sL	2.2	(0.4)	3.1	(0.5)	20.6	(1.6)	51.3	(3.5)	20.3	(3.8)	9.7	(0.9)	1.5	(0.3)	1.25	(0.06)
South Igaliku-1	96 (32)	lS-sL-S	2.9	(0.6)	3.5	(0.5)	18.0	(2.9)	48.4	(8.3)	23.3	(10.8)	7.8	(1.7)	2.2	(0.7)	1.07	(0.14)
South Igaliku-3	72 (24)	sL-lS	3.9	(0.8)	4.4	(1.4)	19.9	(3.2)	43.1	(4.6)	22.8	(7.4)	5.6	(1.5)	3.4	(1.1)	1.05	(0.16)
Igaliku-1	84 (28)	sL	4.4	(0.8)	8.7	(0.7)	22.8	(2.3)	37.2	(4.2)	15.5	(5.8)	3.0	(0.4)	6.6	(1.1)	0.92	(0.11)
Igaliku-2	90 (30)	sL	4.9	(0.7)	9.1	(0.6)	22.6	(1.3)	36.8	(3.0)	16.4	(2.3)	2.8	(0.4)	5.9	(1.0)	0.95	(0.08)
Skellingsted	9 (t*)	lS	5.0	—	2.0	—	6.4	—	23.8	—	61.1	—	3.4	—	1.0	—	1.71	(0.04)
Hjørring	10 (2†)	L-sL	13.6	(2.3)	8.3	(2.9)	24.6	(5.0)	50.6	(10.8)	0.9	(0.4)	2.8	(1.7)	1.1	(0.1)	1.69	(0.08)
Poulstrup sub-soil	18 (2†)	lS	3.8	(0.3)	2.7	(0.3)	11.1	(0.2)	56.0	(0.1)	12.3	(0.2)	9.3	(0.2)	2.3	(0.1)	1.22	(0.06)
Poulstrup top-soil	18 (2†)	ND	ND		ND		ND		ND		ND		ND		10.9	(3.5)	0.59	(0.08)

*transect, † number of sampled soil-horizons (depths)

Table 3 lists the different particle size fractions, along with the number of samples and soil types (Soil Survey Staff, 1999). The sites were grouped according to their land use and ordered with an increasing fine particle content (fines, equivalent particle diameter $D_e < 20\,\mu m$, i.e., the sum of the clay and fine silt fractions) within each group. For better legibility, texture and OC contents in Table 3 were given in $g\,100\,g^{-1}$. Following the definition of TUI, an additional subdivision had to be made within the silt and sand fractions: fine and coarse silt ($2 - 20$ µm and $20 - 50$ µm), and fine and coarse sand ($50 - 200$ µm and $200 - 2000$ µm).

According to Table 3, the cultivated and urban soils generally showed lower OC contents than the pasture or forest soils; the opposite was true for the ρ_b. The field-average ρ_b were non-linearly correlated to OC, as shown in Fig. 2a. We chose to fit a power function to illustrate the non-linear trend between OC and ρ_b, which has been expressed by exponential or reciprocal functions by other studies (Federer et al., 1993; Perie and Ouimet, 2008).

The fS/fines ratio (TUI, texture uniformity index) of the pasture soils exhibited a significant negative linear correlation with OC ($r = -.97^{***}$), and a linear regression based on the pasture soils resulted in a coefficient of determination of $R^2 = .95$, as shown in Fig. 2. The forest soils followed the same linear trend as the pasture soils, whereas only a weak linear correlation between TUI and OC could be observed for the cultivated and urban soils (cultivated soils: $r = -.67^{ns}$), mainly due to the relatively small OC-range of the latter (not shown).

The measured water- and air-phase parameters of all the samples used in this study are shown in Fig. 3: the volumetric water content (θ, $cm^3\,cm^{-3}$), the air-filled porosity (ε,

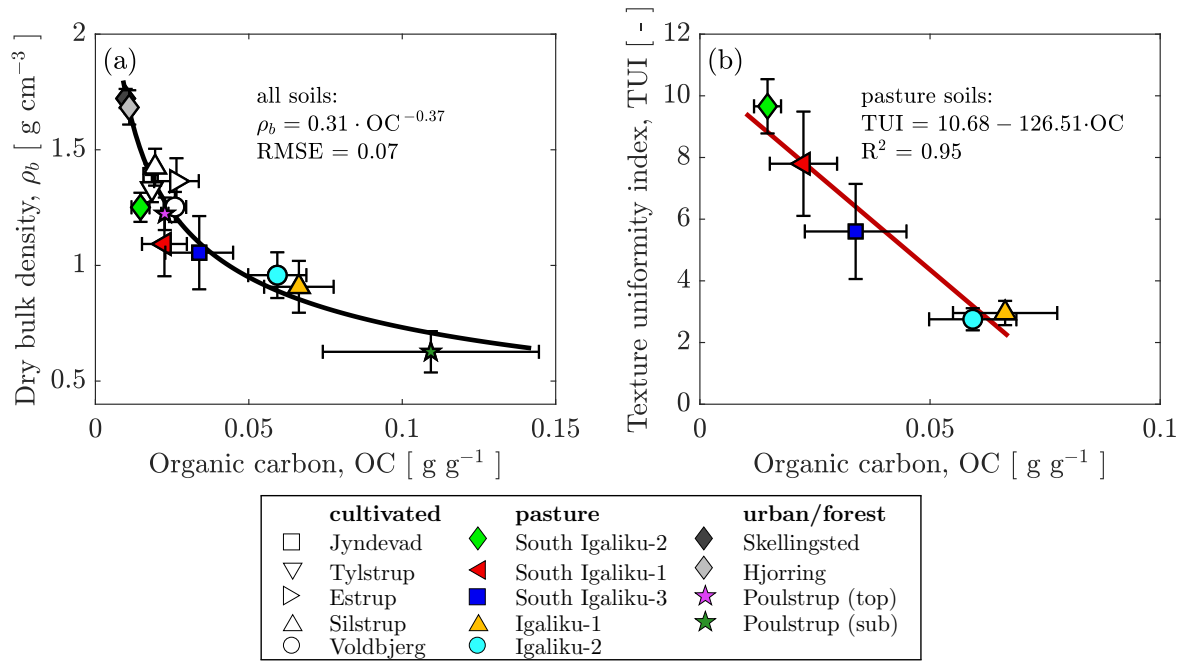

FIGURE 2: (a) The non-linear relation between field-averaged OC and ρ_b. (b) Across-field relation between the OC and the ratio of fine sand to fines (texture uniformity index, TUI) and best linear fit for the pasture soils (5 soils). The symbols are within-field mean values, and the error-bars depict the standard deviation.

cm^3 cm^{-3}), the relative gas-diffusivity (D_p/D_o, dimensionless), and the air-permeability (k_a, µm^2). The abscissa values (pF) of θ and ε in sub-figures Fig. 3a and 3b were shifted randomly within a narrow range [pF ±0.5] around the true pF-value to emphasize the number of measurements per soil-water potential. The used soils spanned a wide range of θ and of ε, and the median θ and ε at each soil-water potential of three selected soils (A: Igaliku-2, sub-arctic pasture, B: Skellingsted, urban and C: Poulstrup-subsoil, temperate forest) were connected by a step-wise linear interpolation polynomial to illustrate the evolution of θ and ε of the three soil-types during drainage. The diffusive and convective mass transport parameters in the gas-phase, D_p/D_o and k_a, respectively, are displayed in Fig. 3c and Fig. 3d. As an illustrative example, the best-fit lines of the D_p/D_o and k_a models (Eq. (4) and Eq. (5)) for the three above-mentioned soils were added to Fig. 3c and Fig. 3d, respectively.

The fitted connectivity-tortuosity parameter, X (Fig. 3c), significantly correlated to ρ_b ($r = -.81^{***}$); furthermore, a linear regression explained 79% of the variation (Fig. 4a). Several other studies (Deepagoda et al., 2011a; Masís-Meléndez et al., 2015) found similar linear correlations between the total porosity or derivations of the latter and X; given the direct linear dependence of Φ on ρ_b, those correlations can be considered as equivalent. Soils showing high X exhibited a more tortuous pore network (Deepagoda et al., 2012), which basically could be traced back to an increase in the amount of parallel and well-connected pores with increasing bulk density, according to Poulsen et al. (2001). In general, the pasture and forest soils showed a more tortuous pore network than the cultivated and urban soils.

The fitted soil-structure index, Ω (Fig. 3d), correlated significantly with the texture uniformity index, TUI (both in log-scale, $r = -.84^{***}$), and a linear regression resulted in a coefficient of determination of $R^2 = .75$ as shown in Fig. 4b. A well-developed soil

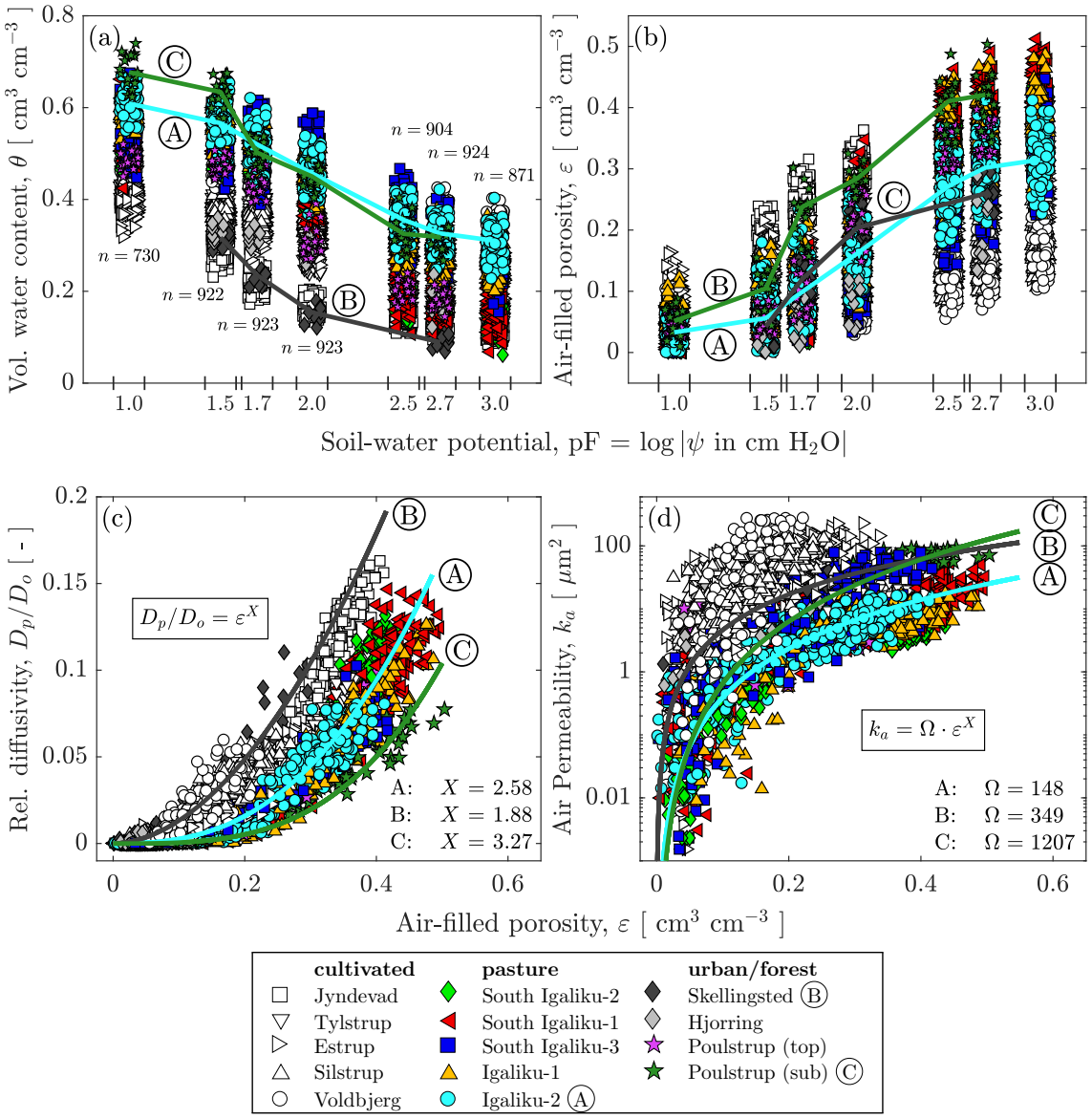

FIGURE 3: Phase distributions and air-phase functions. (a) Volumetric water content, θ, and (b) air-filled porosity, ε, versus soil-water potential levels (pF) and the number of valid measurements per pF (n). The connecting lines for three soils (A: Igaliku-2, B: Skellingsted, C: Poulstrup-sub) are linearly interpolated. (c) Relative diffusivity (D_p/D_o) and applied gas-diffusion model Eq. (4); (d) air permeability (k_a) and applied Ω-model (5) for three selected soils. The parameter Ω was fitted, while X was fixed to the values obtained in sub-figure (c).

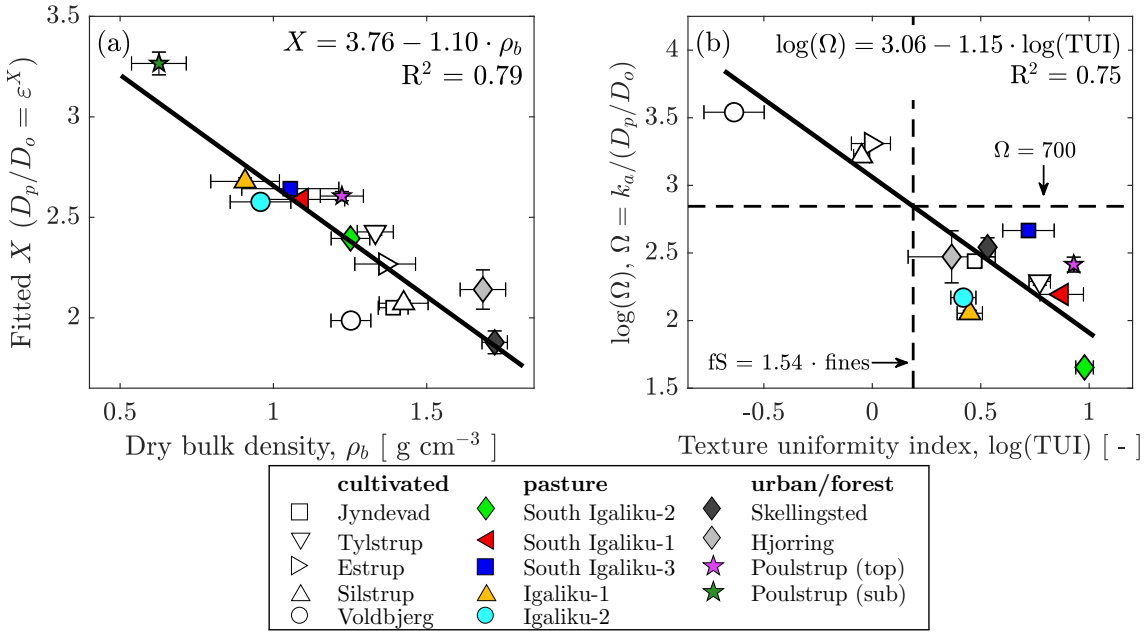

FIGURE 4: (a) Connectivity-tortuosity parameter X (Eq. (4) and Fig. 3c) versus ρ_b and (b) soil-structure index Ω (Eq. (5) and Fig. 3d) as a function of the texture uniformity index TUI (both in log-scale). Dashed horizontal line at the threshold Ω-value for soils exhibiting developed structure. Vertical dashed line depicts the threshold TUI-value at which well-developed soil structure can be expected. Error-bars depict the within-field standard deviation of ρ_b and TUI (horizontal) and the 95% confidence interval of the fitted connectivity-tortuosity parameter X and soil structure parameter Ω (vertical).

structure ($\Omega > 700$) could be observed for soils exhibiting a gravimetric fine sand content smaller than 1.54 times the fine particles content (intersection of the trend-line $\Omega = f(\mathrm{fS/fines})$ and the dashed horizontal line at $\Omega = 700$). The significant correlation suggested that the amount of fine material was a strong driver for soil-structure development. The Greenlandic pasture soils exhibited relatively high fine sand contents compared to the amount of fines, and none of the pasture soils showed signs of well-developed soil structure. The trend-line given in Fig. 4b indicated that the proportionality between D_p/D_o and k_a was highly dependent on the soil's aggregation potential, especially considering the logarithmic scale of both variables.

The considerable effect of compaction (ρ_b) on the air-phase parameters (ε, D_p/D_o, and k_a) is illustrated in Fig. 5. For this purpose, we chose the relatively homogeneous Silstrup field and defined three levels of compaction (low, median, and high), where the degree of compaction was represented by ρ_b. The θ, ε, D_p/D_o, and k_a of each level of compaction was represented by the arithmetic average of the measures of three samples exhibiting the lowest, the closest to the calculated median, and the highest ρ_b, respectively.

The soil-water retention curves at the three levels of compaction, given in Fig. 5a, were only marginally different from each other, whereas the air-filled porosity curves (Fig. 5b) showed considerable differences between each other. The simultaneous look at the water retention and air-filled porosity curves clearly revealed that the differences in available space for gaseous exchange could not be captured by the positions (vertical displacement) of the water retention curves. The ρ_b primarily acts on the total porosity (Φ) and, by that, defining the total void space. The effect of decreasing ρ_b was carried over to the

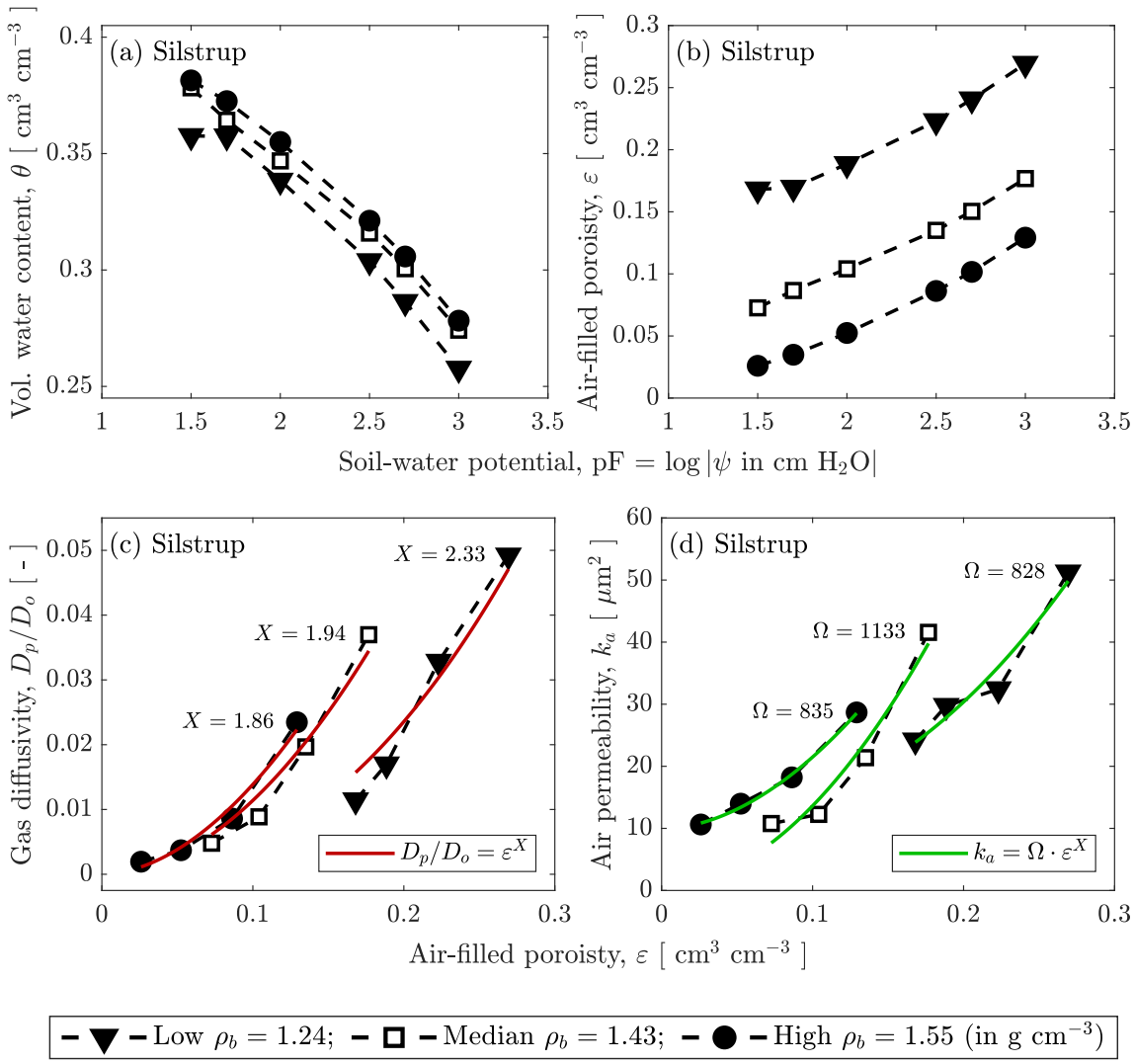

FIGURE 5: Phase distributions and air-phase functions for three levels of natural within-field compaction (Silstrup: low, median, and high ρ_b). (a) Volumetric water content, θ, and (b) air-filled porosity, ε, for wet to dry moisture conditions. Air-phase functions as a function of ε: (c) gas diffusivity (D_p/D_o) and fitted model according to Eq. (4) (fitted connectivity-tortuosity parameter X); (d) air permeability (k_a) and applied Ω-model (Eq. (5)), with fitted structure parameter Ω and fixed X as obtained in sub-figure (c).

air-phase functions via a higher available pore space for gas transport at each moisture level, as shown in Fig. 5c and 5d. It was evident that the within-field variation could not be neglected for either the diffusive or the advective flows.

3.2 Dual-fingerprint for functional soil structure (air space and gas transport)

In the following, the H-model will be applied to investigate further the dependence of ε on ρ_b for different moisture conditions.

3.2.1 Application of the H-model

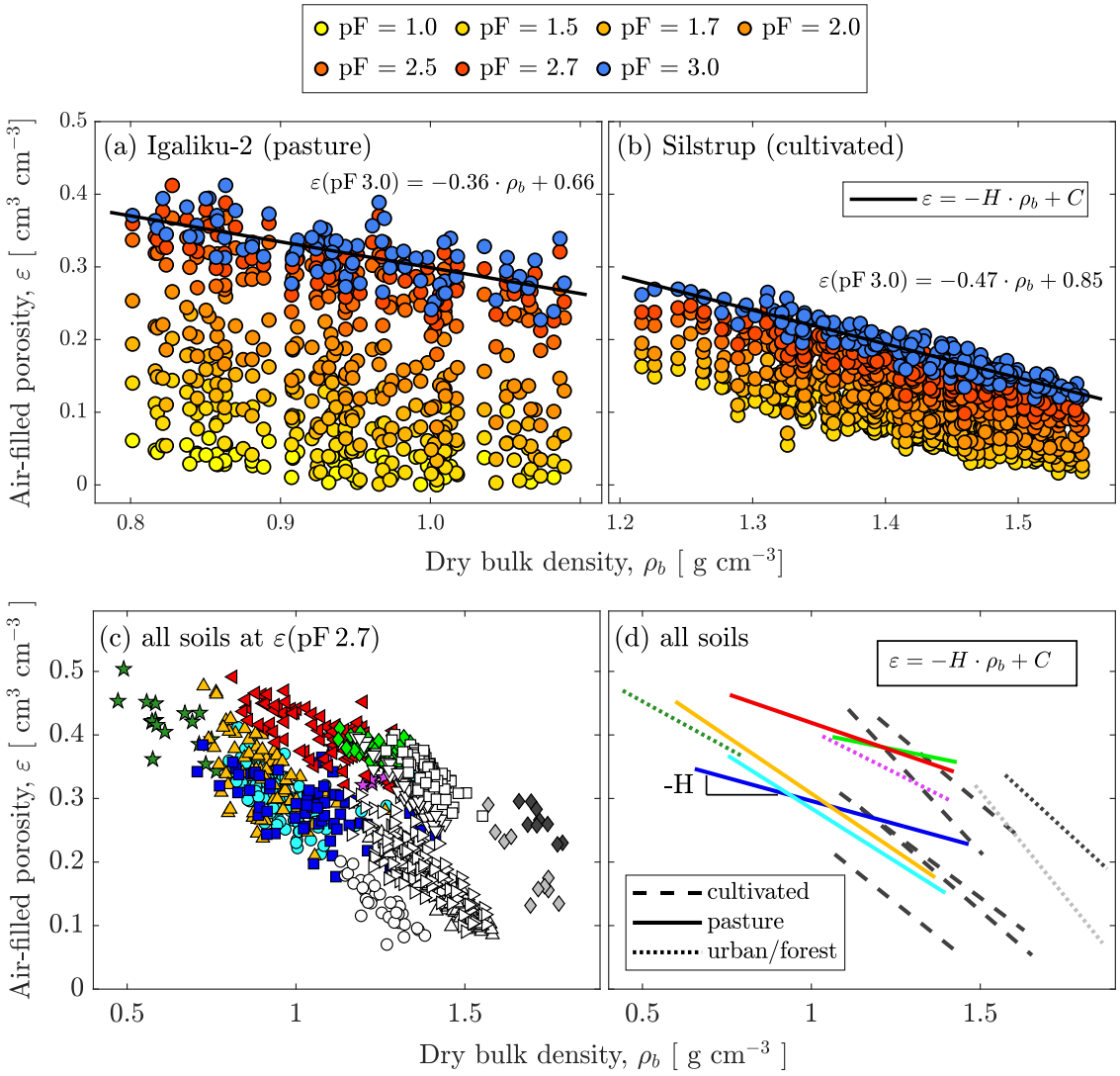

FIGURE 6: Evolution of the air-filled porosity, ε, as a function of dry bulk density, ρ_b, and soil-water potential (pF, color gradient, blue for measurements at pF 3) for a sub-arctic pasture (a) and a temperate cultivated soil (b). Solid lines show the applied H-model (Eq. (1)) at pF 3.0. (c) Scatter plot of ε versus ρ_b at pF 2.7 for the complete data-set and the corresponding H-model for each field (d). Open symbols: cultivated soils; closed colored symbols: pasture and forest soils; closed black and gray symbols: urban soils.

Fig. 6 visualizes the considerable differences in the gradual increase of air-filled porosity

during drainage for two typical soils: a relatively compact and homogeneous, conventionally cultivated temperate soil which was classified as a sandy loam (Silstrup, Denmark) and a perennial pasture soil, which showed considerably lower ρ_b, classified as sandy loam from sub-arctic South Greenland (Igaliku-2, Greenland). Note that no measurements at pF 1.0 of the Silstrup soil were available.
We observed not only an overall dependence of ε on ρ_b, but the different soils also exhibited a different dependence on ρ_b, if subjected to different moisture conditions (e.g., monotonically increasing absolute slope versus variable slope with increasing absolute soil-water potential for Silstrup and Igaliku-2, respectively). As an illustrative example, the H-model (Eq. (1)) was applied to the pairs of measurements at pF 3.0. It is clear from Fig. 6a and Fig. 6b that, although the subarctic pasture soil exhibited significantly lower ρ_b, and therefore a greater Φ than the cultivated sandy loam, the lack of soil-structure and the high tortuosity of the pore network had significant effects on the drainage behavior, especially at lower soil-water potentials (pF $\leq$ 1.7).
The dependencies of ε on ρ_b at pF 2.7 ($\psi = -500\,\mathrm{cm\,H_2O}$) for all the soils used in this study are shown in Fig. 6c, and the applied H-model for the chosen pF-level is displayed in Fig. 6d, as an illustrative example. At pF 2.7, the pores exhibiting a diameter of $D_\phi > 6\,\mu\mathrm{m}$ were drained, according to the capillary rise equation (Schjønning, 1992). The H-model was fitted using a bootstrapped regression scheme to the pairs of (ρ_b, ε) of each soil at each available drainage level, and both, the goodness of fits and significance criteria, were generally high with an increased performance for higher pF. The detailed results of the bootstrapped regression analysis can be found in Table S1 in the appendix.
The main parameter of the H-model (H) reflected the sensitivity of ε to changes in natural compaction, quantified by ρ_b, at a given drainage step. Observing the H index from wet to dry soil conditions enabled to evaluate which faction of the pore size distribution was most vulnerable to changes in ρ_b.

3.2.2 Dual fingerprint

The decadal logarithm of the Kawamoto et al. (2006) soil-structure index, Ω, determined at each soil-water potential level after rearranging Eq. (5) ($\Omega = k_a/(D_p/D_o)$) are given in the left-hand sub-plots of Fig. 7. The dashed horizontal line highlights the threshold value, $\Omega = 700$, in each sub-plot. The right-hand sub-plots of Fig. 7 show the variation of H with the soil-water potential; as a reference for H, the expected H-range for a theoretical pure and uniform sand (see Table 2) was indicated by the shaded area in the plots.
The soils were grouped according to their land use, and the connecting lines were interpolated. The measurements at pF 1.0 were omitted due to the relatively large associated measurement uncertainties at such low suctions.
From a soil-textural perspective, the soil from Jyndevad showed the most narrow and uniform particle-size distribution ($> 80\%$ sand) among the cultivated soils, which was also reflected in its pore-size distribution (Schjønning, 1992; Jensen et al., 2019) and eventually in the range of the calculated H-values, comprised within the boundaries of the expected H-range of pure sands. The relatively low Ω-values (Fig. 7b) throughout the complete moisture range could be associated with the low aggregation potential and non-cohesive nature of the Jyndevad coarse sandy soil (Schjønning, 1992).
The fine sandy Tylstrup soil exhibited considerably higher H-values between pF 1.7 and pF 2.5 than the other cultivated soils, indicating that a change in ρ_b mainly affected the volume of the pore-size classes exhibiting a pore diameter between 10 and 60 µm.

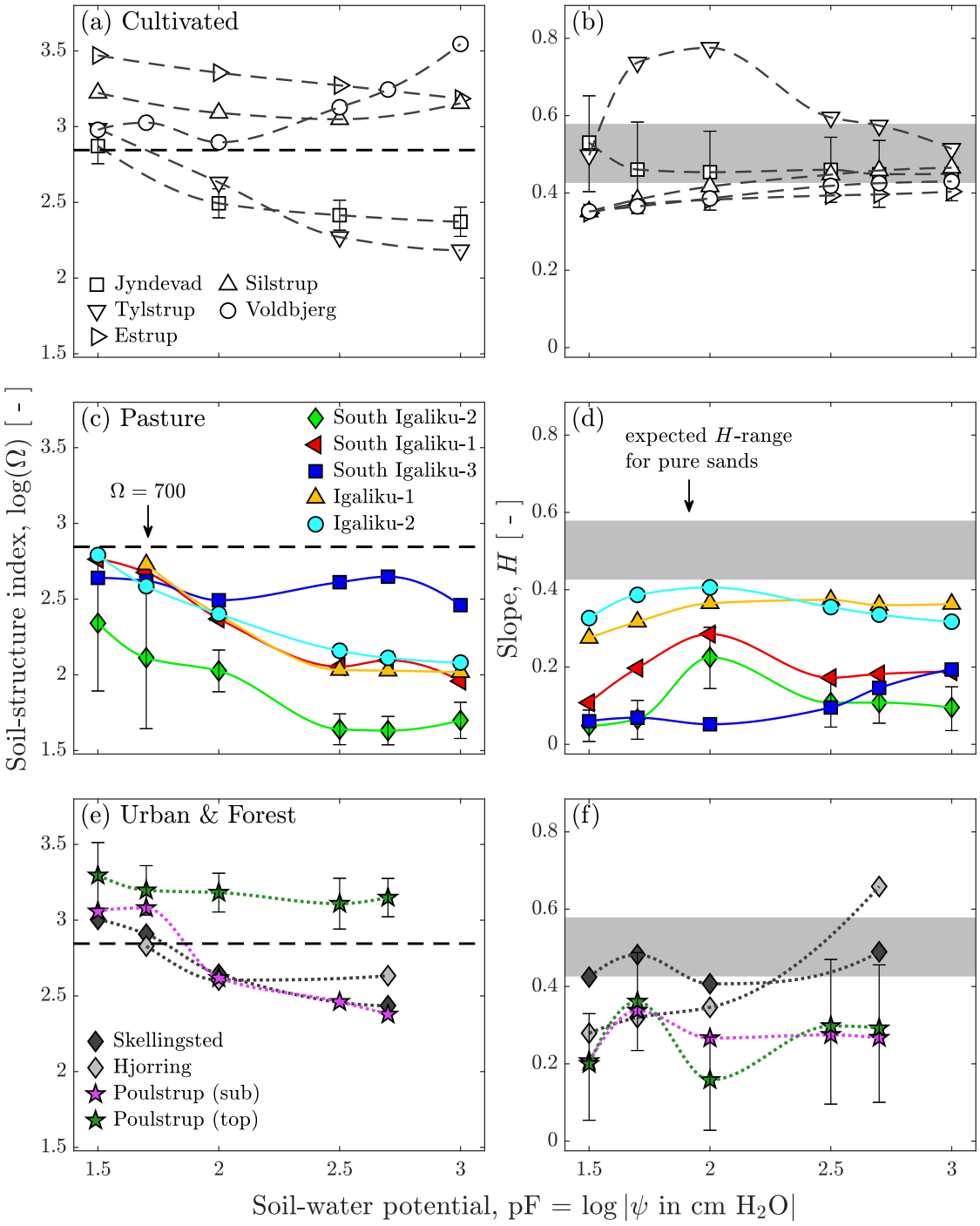

FIGURE 7: The soil-structure index given by the Ω-model (b, d, f) from wet (pF 1.5) to dry (pF 3.0) moisture conditions. The dashed line represents the threshold of $\Omega = 700$ for soil-structure effects on air-phase functional parameters (Kawamoto et al., 2006). The sensitivity of ε to ρ_b (a, c, e) is given by the main parameter of the H-model. The shaded area corresponds to the expected range of H for a pure sand (see Table 2). The error-bars depict the intra-field standard deviation of Ω at each soil-water potential (a, c, e) and the 90% confidence intervals (b, d, f) of H. For better legibility, only one set of error-bars is shown per sub-figure.

Further, the Ω-values below the threshold of $\Omega = 700$ indicated a lack of soil structure for the Tylstrup soils as well.
The finer-grained cultivated soils (Estrup, Silstrup, and Voldbjerg) exhibited a lower H, indicating that the ε at each soil-water potential were less susceptible to changes in ρ_b. The P-values above $\Omega = 700$ throughout the whole moisture range implied the presence of a developed soil structure, i.e., the larger k_a to D_p/D_o ratio indicated a dual-porosity network, exhibiting inter and intra-aggregate porosity, arising from aggregate formation amplified by the relatively high OC and fines contents (Six et al., 1998; Dexter et al., 2008).
The low Ω values of the sandy Jyndevad and Tylstrup soils were a direct consequence of the only marginally differing dominating particle (dispersed particles) sizes compared to the dominating aggregate (non-dispersed) sizes (236 versus 420 µm and 125 versus 250 µm, for the two soils respectively). The Silstup soil on the other hand, showed considerable differences between particle and aggregate sizes (120 versus 6300 µm) (Schjønning, 1992).
The sensitivity of ε to changes in ρ_b of the arctic pasture soils was generally lower (Fig 7c) compared to the temperate cultivated soils, although the low P-values pointed towards a lack of soil structure. Weber et al. (2020) investigated the pore-network connectivity of the herein presented arctic pasture soils and concluded that the pasture soils showed only little to no soil-structure development, which is in accordance with the low Ω-values found in this study.
The forest soils showed H-values similar to the arctic pasture soils. However, the Ω-values of the forest top-soil were consistently higher compared to the pasture soils, mainly due to the low diffusivity compared to the high air permeability of this organic matter-dominated soil. High ε throughout the complete moisture range promoted k_a of the forest top-soil, although D_p/D_o was impeded by the pore-tortuosity presumably created by the high organic matter content (Iiyama and Hasegawa, 2005; Hamamoto et al., 2012). Although the organic matter of the forest soils had not been characterized, it is plausible that it consisted of relatively large amounts of non-decomposed organic matter fragments and a relatively dense root zone. The Greenlandic pasture soils likely exhibited similar characteristics (especially SI-1, SI-2, and SI-3, Pesch et al., 2020), which might be the reason for the similarities between the pasture and forest soils in terms of ρ_b - ε dynamics.
As expected, the samples from Skellingsted, consisting of an artificially compacted, industrial sand cover-layer with low OC, showed H-values in the same order of magnitude as the theoretical sand and the Jyndevad soil. The Hjorring sub-soil samples showed a distinct evolution of H. The high stress at the deeper soil layers caused by the overlying soil probably resulted in a homogeneous pore-size distribution dominated by small pores ($D_\phi \leq 6$ µm) and a shift of high H-values towards smaller pore-sizes (higher pF).
Moldrup et al. (2000a) reported silt-lenses within the soil profile, which most likely had a notable but unspecified effect on the relation between ρ_b and ε. The urban soils showed both relatively low Ω-values, similar to the sandy Jyndevad and Tylstrup soils.

3.3 Two-dimensional, modeled response surface for soil air-filled porosity

3.3.1 Application of the A-model

As shown in the first part of this study, ρ_b could explain the intra-field variation of ε to a large extent, especially at dry soil-conditions. We deployed the earlier introduced A-model (Eq. (2)) to evaluate the within-filed variation of ε for varying moisture

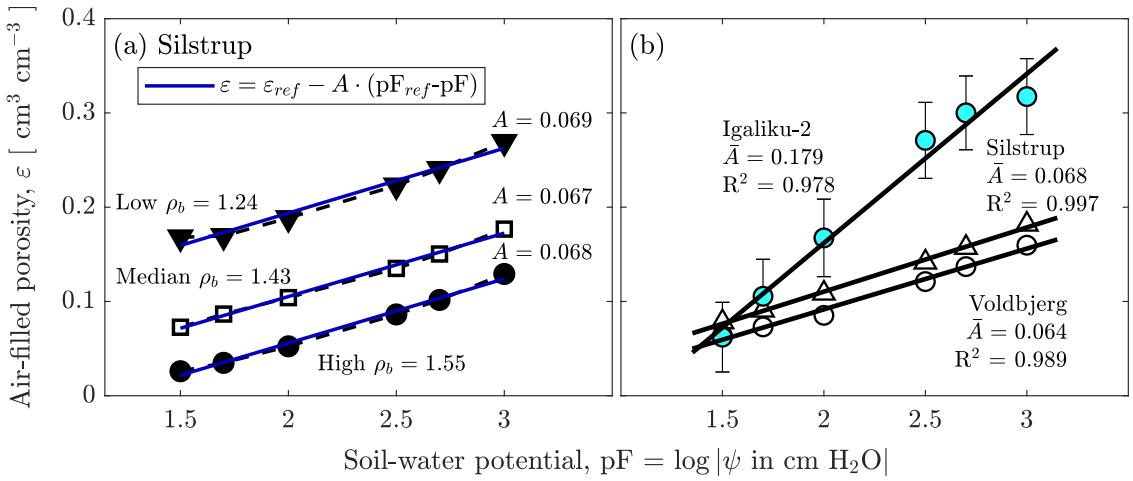

FIGURE 8: Semi-logarithmic soil-air characteristic curve (SL-SAC). Fitted log-linear air-filled porosity model (2) (A-model) to (a) samples from Silstrup, spanning the field's complete ρ_b-range to depict the within-field variation, and to (b) the within-field mean ε of three differently textured soils to depict the across-field variation (error bars depict the standard deviation and are given for one soil only).

conditions. The SL-SAC parameter determined on field-averaged ε were referred to as $\bar{A}$, to avoid confusion with the sample specific A.

The A-model was fitted to ε values measured at soil-water potentials varying between pF 1.5 and pF 3.0, and the reference soil-matric potential was fixed at $\varepsilon_{ref} = \varepsilon(\mathrm{pF}\ 2.7)$. The choice of $\mathrm{pF}_{ref} = 2.7$ was related to data availability; it was the lowest (most negative) soil-water potential at which data was available for all the soils. In principle, pF_{ref} did not necessarily need to be fixed at the highest pF to yield satisfactory regression results. However, the goodness of fit improved markedly for $\mathrm{pF}_{ref} \geq 2$.

The A-model was applied to the measured ε of the same collection of samples from Silstrup as in Fig. 5, covering the complete within-field ρ_b-range (Fig. 8a). As expected, the effect of ρ_b on the sample-specific average ε (horizontal shift of the SL-SAC lines in Fig. 8a) was distinct and also well explained by ρ_b, given the significant correlation between ρ_b and ε(pF 2.7) of $r = -.81^{***}$ or the high explained variation by the linear regression (H-model) given in Table S1 (Silstrup at pF 2.7, $R^2 = .88$).

The performance of the A-model, fitted to the field-averaged ε of three differently textured soils, is displayed in Fig. 8b. The corresponding field-averaged SL-SAC parameters ($\bar{A}$) and R^2 are given in the plot area. The model represented the data of the cultivated loamy to clayey soils fairly well (Silstrup and Voldbjerg), whereas the model could not entirely capture the pronounced curvature of the sandy-loamy pasture soil (Igaliku-2). The $\bar{A}$ of all the 14 soils varied between 0.064 (Voldbjerg) and 0.28 (South-Igaliku 2) and, while being inversely proportional to the gravimetric fines content, a significant linear correlation between $\bar{A}$ and the texture uniformity index, TUI, could be observed ($r = .92^{***}$). Due to the similarity of the A-model to well-known water-retention models, the correlation of the parameter A with TUI was not surprising since other studies found similar correlations between water-retention-model parameters and soil-texture criteria (Clapp and Hornberger, 1978; Vereecken et al., 1989; Pittaki-Chrysodonta et al., 2018).

The dependence of the field-averaged A-model parameter on basic soil properties was

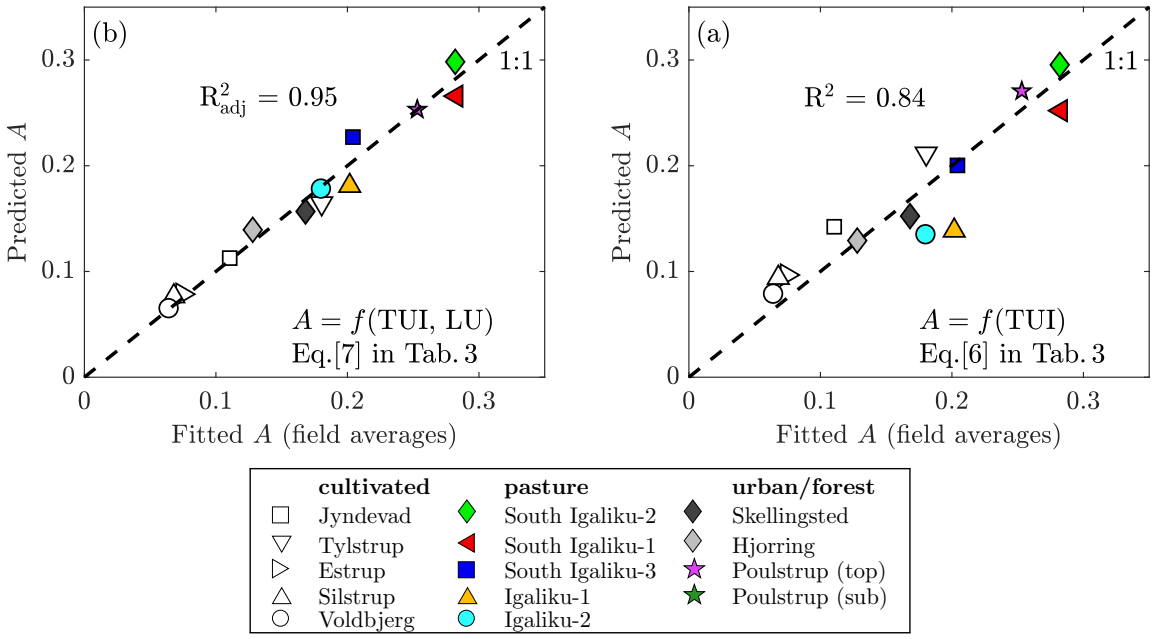

FIGURE 9: Prediction of the field-averaged SL-SAC parameter $\bar{A}$ by: (a) linear regression with the texture uniformity index, TUI (fS/fines), and (b), including the land use index, LU, as predictors; detailed statistics in Tab. 4; no texture data for Poulstrup (top).

TABLE 4: Results of the linear regressions to predict the field-averaged SL-SAC parameter $\bar{A}$. (7) with the texture uniformity index, TUI, as independent variable; (8) additionally including a factor accounting for land use (LU†). n, number of observations included in the regression; R^2 and R^2_{adj}, ordinary and adjusted coefficient of determination, respectively; RMSE, root-mean-square error; AICc, Akaike information criterion adjusted for small sample numbers; exponents of regression coefficients depict the significance levels according to the rules given in the methods section.

		Model	n	R^2/$^\ddagger R^2_{adj}$	RMSE	AICc
(7)	Fig.9a	$A = 0.073^{**} + 0.024^{***} \cdot$ (TUI)	13	0.844	0.032	-49.83
(8)	Fig.9b	$A = 0.061^{**} + 0.017^{***} \cdot$ (TUI)	13	‡0.955	0.016	-57.88
		$+ 0.071 \cdot$ #pasture†				
		$+0.036 \cdot$ #urban†				
		$+0.044 \cdot$ #forest†				

† LU is expressed explicitly, omitting the reference level #cultivated, as: #pasture takes the value 1 if the land use is pasture and 0 if not, same for #urban and #forest.

evaluated via linear regressions, and it could be accurately predicted by a regression including the texture uniformity parameter, TUI (Fig. 9a and Eq. (7)). However, including a nominal categorical variable accounting for the land uses (LU:= {cultivated, pasture, urban, forest}) increased the explained variation from 86% to 98% and the model performance by more than 20% compared to the initial model (Fig. 9b and Eq. (8)). The analysis of variance of the regression model (Eq. (8)) showed that the categorical variable was significant at the 1% significance level (LU: $p(> F) = .003$). Significant collinearity among the predictors could be safely rejected because of the invertibility of the predictor matrix. The effect of the land use on the marginal means of the

LU-grouped A compared to the reference level given by the mean A of the cultivated soils was given explicitly in the model function Eq. (8) in Table 4 (regression coefficients associated with the levels of the categorical factor).
The outcome of the multiple linear regressions revealed that the variation of the across-field $\bar{A}$ was explained by the LU factor at a precision-level, which could not be achieved by ρ_b and TUI alone (not significant ρ_b, if included in the regression, not shown), indicating that the LU-factor incorporated information which was not captured by the continuous independent variables.
From the linear regressions established in the first part of the study, ε could be accurately predicted from ρ_b, so that, it was possible to predict the complete soil-air characteristic curve for any ρ_b by combining the H- and A-models.

3.3.2 Modeled response surface (MRS)

TABLE 5: Fitted and estimated values to compute the response plane in Fig. 10 from the A-model (to estimate A) in combination with the H-model (to estimate ε_{ref}). The measured (fitted) variables (ε_{ref} and $\bar{A}$, both field-averages) are given as reference. The error of the estimated ε using the MRS-model compared to the measured ε at three ρ_b-levels is given by the RMSE.

Site	H	ε_{ref}		$\bar{A}$		RMSE(ε)		
	fitted	measured	$f(H, \tilde{\rho}_b)$	fitted	f(TUI, LU)	low ρ_b	median ρ_b	high ρ_b
Igaliku-2	0.336	0.302	0.304	0.180	0.179	0.021	0.023	0.015
Silstrup	0.458	0.157	0.154	0.068	0.077	0.011	0.010	0.013

The expression for ε_{ref} in the A-model (Eq. (2), reference fixed at pF 2.7)) was substituted by the H-model (Eq. (1)), which permitted the generation of a modeled response surface (MRS, Eq. (3)). The SL-SAC parameter A was estimated from the linear model (Eq. (8)) with field-average TUI and LU as predictors.
The estimated ε for simulated ρ_b, spanning the soils ρ_b-range and from wet to dry soil conditions for Igaliku-2 and Silstrup, are shown in Fig. 10. Negative outputs were set to null. The fitted and estimated parameter inputs are given in Table 5; the relevant H were obtained from Table S1 (H(pF 2.7) for Igaliku-2 and Silstrup, respectively).
The A-model, in combination with the H-model, could thus accurately predict the ε for samples exhibiting a wide ρ_b-range for wet to dry conditions. To be able to predict the air-characteristic curve completely from texture and land use, a prediction model for the parameter H would be needed. It can be shown that H can be very accurately predicted from the gravimetric OC and fine sand ($D_e < 200\,\mu m$) contents, along with the LU factor ($R^2_{adj} = .94$, not shown).
However, the nominal land-use variable, LU, differentiated not only between the different land uses but also between the climatic regions (arctic and temperate) and most likely included hidden components that influenced the ε evolution during drainage.
Additionally, the sample sizes between the different land-use groups differed to such an extent that a reliable, unbiased prediction model could not be established. In order to avoid a gray-box and heavily biased model, it was preferred not to elaborate further on the prediction model at this time.
The concept map given in Fig. 10a elucidates the relations between the different controls (texture, compaction, and land use) and the resulting soil structure fingerprints and final response surface for ε. Organic matter was not used as a control parameter; however,

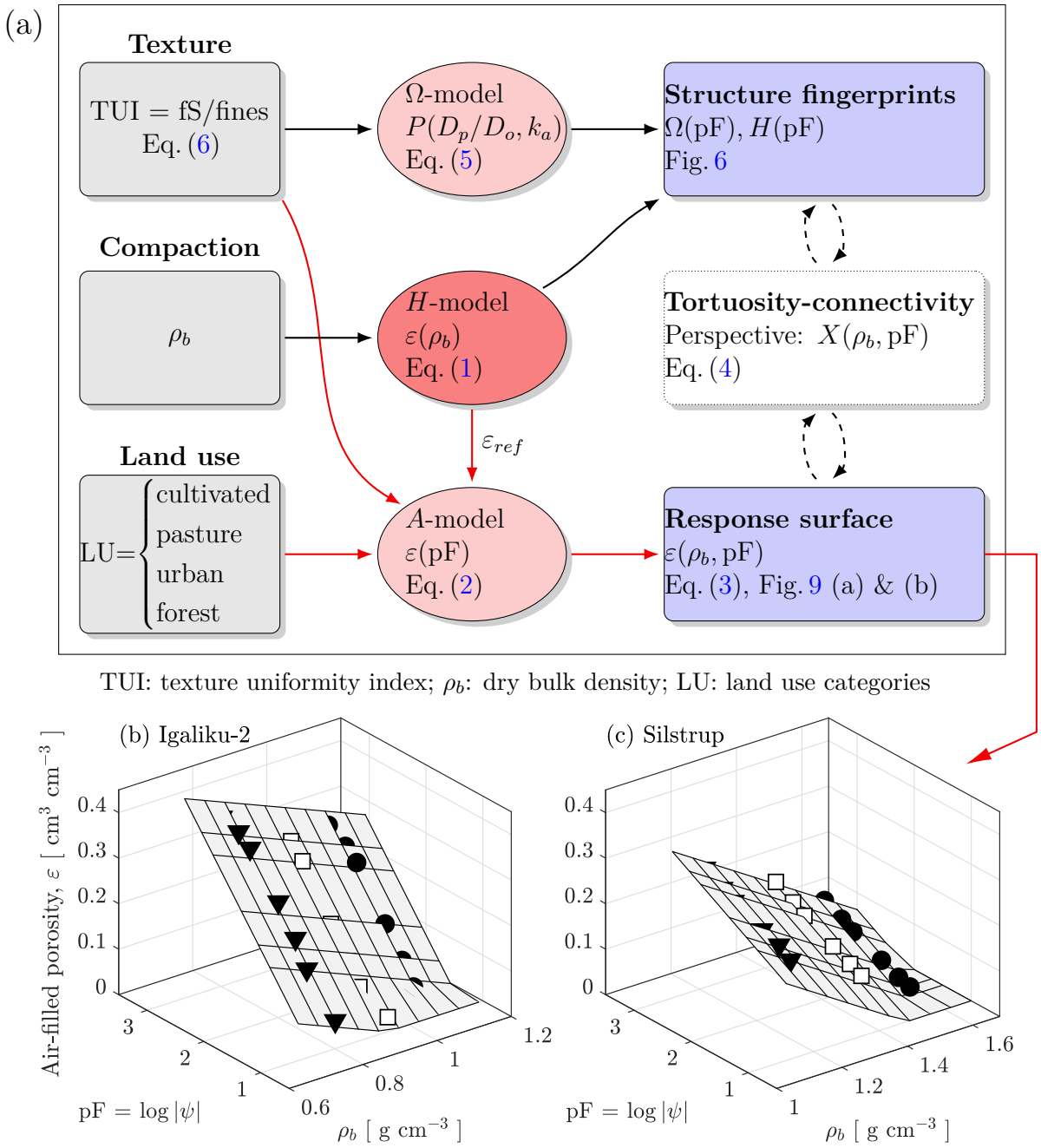

FIGURE 10: (a) Relational concept map elucidating the connections between soil state variables (texture, compaction, and land use), the deployed models, and the resulting descriptive entities. Estimated ε for varying ρ_b and pF. Symbols: measured ε corresponding to lowest (▼), median (□) and highest (●) ρ_b of (b) Igaliku-2 and (c) Silstrup. Plane: estimated ε from *A*-model (2) in combination with the *H*-model (1) for simulated ρ_b spanning the ρ_b-range of the two selected fields. Model parameters and relative error (RMSE) are given in Table 5.

from Fig. 2, it was apparent that OC was strongly connected to TUI and ρ_b. Furthermore, many studies have shown that the quantity and quality of the organic matter fractions are ultimately controlled by land use (Parfitt et al., 1997; Leifeld and Kögel-Knabner, 2005; Yeasmin et al., 2020) and, also, have a distinct effect on the air-phase functions (Resurreccion et al., 2007). Especially in regard to climate and potential land-use changes

at high latitudes, the effect on the organic matter pools and subsequent changes in soil structure and related soil-functional parameters and gas-exchange processes may eventually be modeled and simulated by the combination of the presented soil-structure fingerprints (Ω(pF) and H(pF)) and simple ε-response surface via the connectivity-tortuosity factor X, which, in turn, was shown to be correlated to ρ_b (Fig. 4).

4 Conclusion

From comprehensive soil physical data measured at different moisture conditions on 14 different soils representing four different land uses, two climatic zones, and a wide range of soil texture and bulk density (ρ_b), we conclude:

1. Bulk density (ρ_b) was strongly and non-linearly related to organic matter (OC) across the fields, but only weakly within the fields for some of the South Greenlandic pastures. The ratio of fine sand to fines, referred to as the texture uniformity index (TUI), exhibited different relations with OC across the land uses and climate zones.

2. The connectivity-tortuosity parameter, X, was significantly negatively correlated to ρ_b, whereas, on the other hand, the soil-structure index, Ω, was significantly negatively correlated to the TUI. For the herein used soils, no signs of structure development were observed for the pasture soils.

3. The simultaneous display of the soil-water retention curve (WRC, volumetric water content, θ) along with the soil-air characteristic curve (SAC, air-filled porosity, ε) revealed that the SAC varied significantly for varying levels of compaction, whereas the WRC varied only marginally. The air-phase functions (relative diffusivity and air permeability, D_p/D_o and k_a, respectively) showed relatively large variations along the ρ_b-gradient, mainly due to the considerable effect of ρ_b on ε, and hence on the available void-space for gaseous exchanges.

4. The air-filled porosity (ε) of the different soils exhibited distinct linear dependencies on ρ_b at changing moisture conditions. The slopes, H, of these linear dependencies (H-model) showed different magnitudes for contrasting soil-types and land uses. The H-parameter, interpreted as a measure of the sensitivity of ε to changes in ρ_b, revealed that the ε at each pF of the subarctic pasture soils were less sensitive to changes in ρ_b than similarly textured cultivated soils.

5. The soil-structure index, Ω, calculated as the ratio of k_a to D_p/D_o for each soil-water potential level, enabled to differentiate between the textures of the cultivated soils. The pasture soils, on the other hand, did not show signs of a developed soil structure.

6. The semi-logarithmic soil-air characteristic curve could be reasonably well described by the developed A-model (2 parameters: A and ε_{ref}). For the herein used soils, the model parameter, A, could be accurately predicted by the TUI and a factor accounting for environmental properties, including land use, achieving a coefficient of determination of $R^2 = .95$.

7. The combination of the H-model (to estimate ε_{ref}) and the A-model (to simulate the response of ε to changes in pF) was successfully applied to model a response surface of ε as a function of ρ_b and pF (MRS).

The dry bulk density, ρ_b, turned out to be the chief parameter explaining the within-field variation of ε, and thus, to a large extent, also the levels of air-exchange processes within a field. On the contrary, the across-field variation was better explained by texture together with a categorical factor accounting for environment-specific properties (including land use and management). The effect size of ρ_b on the field-averaged ε was statistically less significant than texture and environmental factors.
In perspective and towards actual use, the MRS-concept should be further tested, validated against independent data, and extended to include non-linear ε-pF models. The combined controls of soil compaction (density), type (texture), and environmental factors, including land-use, on the three air-phase parameters (ε, D_p/D_o, and k_a) will be a key to predict future changes in soil ecosystem services.

Conflict of interest

The authors declare that there is no conflict of interest.

Funding

The research was financed by the Danish Council for Independent Research, Technology, and Production Sciences via the project "Glacial Flour as a New, Climate-Positive Technology for Sustainable Agriculture in Greenland: NewLand".

Orchid

Charles Pesch: https://orcid.org/0000-0003-4120-0239

Supplemental Material S Regression table

The supplemental material consists of one table (three parts) containing the statistics of the bootstrapped regression of the H-model.

References

Annabi, M., Le Bissonnais, Y., Le Villio-Poitrenaud, M., Houot, S., 2011. Improvement of soil aggregate stability by repeated applications of organic amendments to a cultivated silty loam soil. Agriculture, Ecosystems & Environment 144 (1), 382–389.

Arthur, E., Moldrup, P., Schjønning, P., de Jonge, Lis, W., Jan. 2012. Linking particle and pore size distribution parameters to soil gas transport properties. Soil Science Society of America Journal 76 (1), 18–27.

Arya, L. M., Paris, J. F., 1981. A physicoempirical model to predict the soil moisture characteristic from particle-size distribution and bulk density data. Soil Science Society of America Journal 45 (6), 1023–1030.

Assouline, S., Tuli, A., Hopmans, J. W., 2016. Evaluating the relative air permeability of porous media from their water retention curves. Water Resources Research 52 (5), 3428–3439.

Ball, B. C., 1981. Modelling of soil pores as tubes using gas permeabilities, gas diffusivities and water release. Journal of Soil Science 32 (4), 465–481.

Ball, B. C., 2013. Soil structure and greenhouse gas emissions: a synthesis of 20 years of experimentation. European Journal of Soil Science 64 (3), 357–373.

Ball, B. C., Campbell, D. J., Douglas, J. T., Henshall, J. K., O'Sullivan, M. F., 1997. Soil structural quality, compaction and land management. European Journal of Soil Science 48 (4), 593–601.

Ball, B. C., Schjønning, P., 2002. 4.4 Air Permeability. In: Dane, J. H., Topp, C. G. (Eds.), Methods of Soil Analysis: Part 4 Physical Methods. No. 5.4 in SSSA Book Series. Soil Science Society of America, Madison, WI, pp. 1141–1158.

Bottinelli, N., Angers, D. A., Hallaire, V., Michot, D., Le Guillou, C., Cluzeau, D., Heddadj, D., Menasseri-Aubry, S., 2017. Tillage and fertilization practices affect soil aggregate stability in a Humic Cambisol of northwest France. Soil and Tillage Research 170, 14–17.

Buckingham, E., 1904. Contributions to our knowledge of the aeration of soils. Tech. Rep. 25, Bureau of Soils, US Deptartment of Agriculture, Washington.

Campbell, G. S., 1974. A simple method for determining unsaturated conductivity from moisture retention data. Soil Science 117 (6), 311–314.

Cannon, W. A., Free, E. E., 1917. The ecological significance of soil aeration. Science 45 (1156), 178–180.

Cappelen, J., 2019. Guide to climate data and information from the Danish Meteorological Institute. Tech. Rep. 19-10, DMI, Danish Meteorological Institute, Copenhagen, from http://www.dmi.dk/dmi/tr19-10 (visited online: August 30, 2021).

Carlson, A. E., Winsor, K., Ullman, D. J., Brook, E. J., Rood, D. H., Axford, Y., LeGrande, A. N., Anslow, F. S., Sinclair, G., 2014. Earliest Holocene south Greenland ice sheet retreat within its late holocene extent. Geophysical Research Letters 41 (15), 5514–5521.

Chesters, G., Attoe, O. J., Allen, O. N., 1957. Soil aggregation in relation to various soil constituents. Soil Science Society of America Journal 21 (3), 272–277.

Clapp, R. B., Hornberger, G. M., 1978. Empirical equations for some soil hydraulic properties. Water Resources Research 14 (4), 601–604.

Currie, A. J., 1960a. Gaseous diffusion in porous media. Part 1. - A non-steady state method. British Journal of Applied Physics 11 (8), 314–317.

Currie, A. J., 1960b. Gaseous diffusion in porous media. Part 2. - Dry granular materials. British Journal of Applied Physics 11 (8), 318–324.

Currie, J. A., 1961. Gaseous diffusion in porous media. Part 3 - Wet granular materials. British Journal of Applied Physics 12 (6), 275–281.

Dane, J. H., Hopmans, J. W., 2002. 3.1 Water Content. In: Dane, J. H., Topp, C. G. (Eds.), Methods of Soil Analysis: Part 4 Physical Methods. Vol. 4 of 5. Soil Science Society of America, Madison, WI, pp. 417–545.

Deepagoda, T. K. K. C., Moldrup, P., Schjønning, P., de Jonge, L. W., Kawamoto, K., Komatsu, T., 2011a. Density-corrected models for gas diffusivity and air permeability in unsaturated soil. Vadose Zone Journal 10 (1), 226–238.

Deepagoda, T. K. K. C., Moldrup, P., Schjønning, P., Kawamoto, K., Komatsu, T., de Jonge, L. W., 2011b. Generalized density-corrected model for gas diffusivity in variably saturated soils. Soil Science Society of America Journal 75 (4), 1315–1329.

Deepagoda, T. K. K. C., Moldrup, P., Schjønning, P., Kawamoto, K., Komatsu, T., de Jonge, L. W., 2012. Variable pore connectivity model linking gas diffusivity and air-phase tortuosity to soil matric potential. Vadose Zone Journal 11 (1).

Dexter, A. R., Richard, G., Arrouays, D., Czyż, E. A., Jolivet, C., Duval, O., 2008. Complexed organic matter controls soil physical properties. Geoderma 144 (3), 620–627.

Dlapa, P., Hriník, D., Hrabovský, A., Šimkovic, I., Žarnovičan, H., Sekucia, F., Kollár, J., 2020. The impact of land-use on the hierarchical pore size distribution and water retention properties in loamy soils. Water 12 (2).

Dörner, J., Dec, D., Thiers, O., Paulino, L., Zúñiga, F., Valle, S., Martínez, O., Horn, R., 2016. Spatial and temporal variability of physical properties of Aquands under different land uses in southern Chile. Soil Use and Management 32 (3), 411–421.

Eden, M., Schjønning, P., Moldrup, P., De Jonge, L. W., 2011. Compaction and rotovation effects on soil pore characteristics of a loamy sand soil with contrasting organic matter content. Soil Use and Management 27 (3), 340–349.

Efron, B., 1979. Bootstrap methods: Another look at the jackknife. Annals of Statistics 7 (1), 1–26.

Efron, B., 1983. Estimating the error rate of a prediction rule: improvement on cross-validation. Journal of the American Statistical Association 78 (382), 316–331.

Egli, M., Hunt, A. G., Dahms, D., Raab, G., Derungs, C., Raimondi, S., Yu, F., 2018. Prediction of soil formation as a function of age using the percolation theory approach. Frontiers in Environmental Science 6, 108.

Federer, C. A., Turcotte, D. E., Smith, C. T., 1993. The organic fraction–bulk density relationship and the expression of nutrient content in forest soils. Canadian Journal of Forest Research 23 (6), 1026–1032.

Folkoff, M. E., Meentemeyer, V., 1987. Climatic control of the geography of clay minerals genesis. Annals of the Association of American Geographers 77 (4), 635–650.

Gee, G. W., Or, D., 2002. 2.4 Particle-Size Analysis. In: Dane, J. H., Topp, C. G. (Eds.), Methods of Soil Analysis: Part 4 Physical Methods. Vol. 4 of 5. Soil Science Society of America, Madison, WI, pp. 255–293.

Gregorich, E. G., Rochette, P., VandenBygaart, A. J., Angers, D. A., 2005. Greenhouse gas contributions of agricultural soils and potential mitigation practices in Eastern Canada. Soil and Tillage Research 83 (1), 53–72.

Gregson, K., Hector, D. J., McGowan, M., 1987. A one-parameter model for the soil water characteristic. Journal of Soil Science 38 (3), 483–486.

Hamamoto, S., Moldrup, P., Kawamoto, K., Komatsu, T., 2012. Organic matter fraction dependent model for predicting the gas diffusion coefficient in variably saturated soils. Vadose Zone Journal 11 (1).

Hermansen, C., Knadel, M., Moldrup, P., Greve, M. H., Karup, D., de Jonge, L. W., 2017. Complete soil texture is accurately predicted by visible near-infrared spectroscopy. Soil Science Society of America Journal 81 (4), 758–769.

Iiyama, I., Hasegawa, S., 2005. Gas diffusion coefficient of undisturbed peat soils. Soil Science and Plant Nutrition 51 (3), 431–435.

Iversen, V., B., Moldrup, V., P., Schjønning, V., P., Loll, V., P., 2001. Air and water permeability in differently textured soils at two measurement scales. Soil Science 166 (10), 643–659.

Jensen, J. L., Schjønning, P., Watts, C. W., Christensen, B. T., Munkholm, L. J., 2019. Soil water retention: Uni-modal models of pore-size distribution neglect impacts of soil management. Soil Science Society of America Journal 83 (1), 18–26.

Johnson, J. M.-F., Franzluebbers, A. J., Weyers, S. L., Reicosky, D. C., 2007. Agricultural opportunities to mitigate greenhouse gas emissions. Environmental Pollution 150 (1), 107–124.

Karup, D., Moldrup, P., Paradelo, M., Katuwal, S., Norgaard, T., Greve, M. H., de Jonge, L. W., 2016. Water and solute transport in agricultural soils predicted by volumetric clay and silt contents. Journal of Contaminant Hydrology 192, 194 – 202.

Katuwal, S., Arthur, E., Tuller, M., Moldrup, P., de Jonge, L. W., 2015. Quantification of soil pore network complexity with X-ray computed tomography and gas transport measurements. Soil Science Society of America Journal 79 (6), 1577–1589.

Kawamoto, K., Moldrup, P., Schjønning, P., Iversen, B. V., Komatsu, T., Rolston, D. E., 2006. Gas transport parameters in the vadose zone: Development and tests of power-law models for air permeability. Vadose Zone Journal 5 (4), 1205–1215.

Kerr, P. F., 1952. Formation and occurrence of clay minerals. Clays and Clay Minerals 1 (1), 19–32.

Kruse, C. W., Moldrup, P., Iversen, N., 1996. Modeling diffusion and reaction in soils. II. Atmospheric methane diffusion and consumption in a forest soil. Soil science 161 (6), 355–365.

Leifeld, J., Kögel-Knabner, I., 2005. Soil organic matter fractions as early indicators for carbon stock changes under different land-use? Geoderma 124 (1), 143–155.

Li, Z., Zhang, X., Liu, Y., 2017. Pore-scale simulation of gas diffusion in unsaturated soil aggregates: Accuracy of the dusty-gas model and the impact of saturation. Geoderma 303, 196–203.

Lindhardt, B., Abildtrup, C., Vosgerau, H., Olsen, P., Torp, S., Iversen, B. V., Jørgensen, J. O., Plauborg, F., Rasmussen, P., Gravesen, P., 2001. The Danish pesticide leaching assessment programme. Site characterization and monitoring design, GEUS, Copenhagen, Denmark.

Lipiec, J., Hajnos, M., Świeboda, R., 2012. Estimating effects of compaction on pore size distribution of soil aggregates by mercury porosimeter. Geoderma 179-180, 20–27.

Masís-Meléndez, F., Chamindu Deepagoda, T. K. K., de Jonge, L. W., Tuller, M., Moldrup, P., 2014. Gas diffusion-derived tortuosity governs saturated hydraulic conductivity in sandy soils. Journal of Hydrology 512, 388–396.

Masís-Meléndez, F., de Jonge, L. W., Chamindu Deepagoda, T. K. K., Tuller, M., Moldrup, P., 2015. Effects of soil bulk density on gas transport parameters and pore-network properties across a sandy field site. Vadose Zone Journal 14 (7), 1–12 vzj2014.09.0128.

MATLAB and Statistics Toolbox, 2018. version 9.5.0 (R2018b). The MathWorks Inc., Natick, Massachusetts.

Millington, R. J., Quirk, J. M., 1964. Formation factor and permeability equations. Nature 202, 143–145.

Millington, R. J., Quirk, J. P., 1961. Permeability of porous solids. Transactions of the Faraday Society 57, 1200–1207.

Moldrup, P., Kruse, C. W., Rolston, D. E., Yamaguchi, T., 1996. Modeling diffusion and reaction in soils. III. Predicting gas diffusivity from the Campbell soil-water retention model. Soil science 161 (6), 366–375.

Moldrup, P., Olesen, T., Gamst, J., Schjønning, P., Yamaguchi, T., Rolston, D. E., 2000a. Predicting the gas diffusion coefficient in repacked soil: Water-induced linear reduction model. Soil Science Society of America Journal 64 (5), 1588–1594.

Moldrup, P., Olesen, T., Schjønning, P., Yamaguchi, T., Rolston, D. E., 2000b. Predicting the gas diffusion coefficient in undisturbed soil from soil water characteristics. Soil Science Society of America Journal 64 (1), 94–100.

Moldrup, P., Olesen, T., Yamaguchi, T., Schjønning, P., Rolston, D. E., 1999. Modeling diffusion and reaction in soils: IX. The Buckingham-Burdine-Campbell equation for gas diffusivity in undisturbed soil. Soil science 164 (8), 542–551.

Moldrup, P., Olesen, T., Yoshikawa, S., Komatsu, T., Rolston, D. E., 2004. Three-porosity model for predicting the gas diffusion coefficient in undisturbed soil. Soil Science Society of America Journal 68 (3), 750–759.

Moldrup, P., Yoshikawa, S., Olesen, T., Komatsu, T., Rolston, D. E., 2003a. Air permeability in undisturbed volcanic ash soils. Soil Science Society of America Journal 67 (1), 32–40.

Moldrup, P., Yoshikawa, S., Olesen, T., Komatsu, T., Rolston, D. E., 2003b. Gas diffusivity in undisturbed volcanic ash soils. Soil Science Society of America Journal 67 (1), 41–51.

Nielsen, J. E., Karup, D., De Jonge, L. W., Ahm, M., Bentzen, T. R., Rasmussen, M. R., Moldrup, P., 9 2018. Can the volume ratio of coarse to fine particles explain the hydraulic properties of sandy soil? Soil Science Society of America Journal 82 (5), 1093–1100.

Norgaard, T., Moldrup, P., Olsen, P., Vendelboe, A. L., Iversen, B. V., Greve, M. H., Kjaer, J., de Jonge, L. W., 2013. Comparative mapping of soil physical–chemical and structural parameters at field scale to identify zones of enhanced leaching risk. Journal of Environmental Quality 42 (1), 271–283.

Paradelo, M., Norgaard, T., Moldrup, P., Ferré, T. P. A., Kumari, K. G. I. D., Arthur, E., de Jonge, L. W., 2015. Prediction of the glyphosate sorption coefficient across two loamy agricultural fields. Geoderma 259-260, 224–232.

Parfitt, R. L., Theng, B. K. G., Whitton, J. S., Shepherd, T. G., 1997. Effects of clay minerals and land use on organic matter pools. Geoderma 75 (1), 1–.12.

Perie, C., Ouimet, R., 2008. Organic carbon, organic matter and bulk density relationships in boreal forest soils. Canadian Journal of Soil Science 88 (3), 315–325.

Pesch, C., Lamandé, M., de Jonge, L. W., Norgaard, T., Greve, M. H., Moldrup, P., 2020. Compression and rebound characteristics of agricultural sandy pasture soils from South Greenland. Geoderma 380, 114608.

Pesch, C., Weber, P. L., de Jonge, L. W., Greve, M. H., Norgaard, T., Moldrup, P., 2021. Soil–air phase characteristics: Response to texture, density, and land use in Greenland and Denmark. Soil Science Society of America Journal, 1–21.

Pittaki-Chrysodonta, Z., Moldrup, P., Knadel, M., Iversen, B. V., Hermansen, C., Greve, M. H., de Jonge, L. W., 2018. Predicting the Campbell soil water retention function: Comparing visible–near-infrared spectroscopy with classical pedotransfer function. Vadose Zone Journal 17 (1), 170169.

Poulsen, T. G., Christophersen, M., Moldrup, P., Kjeldsen, P., 2001. Modeling lateral gas transport in soil adjacent to old landfill. Journal of Environmental Engineering 127 (2), 145–153.

Poulsen, T. G., Moldrup, P., Yamaguchi, T., Massmann, J. W., Hansen, J. A., 1998. VOC vapor sorption in soil: Soil type dependent model and implications for vapor extraction. Journal of Environmental Engineering 124 (2), 146–155.

Poulsen, T. G., Moldrup, P., Yamaguchi, T., Schjønning, P., Hansen, J. A., 1999. Predicting soil-water and soil-air transport properties and their effects on soil-vapor extraction efficiency. Groundwater Monitoring & Remediation 19 (3), 61–70.

Resurreccion, A. C., Kawamoto, K., Komatsu, T., Moldrup, P., Sato, K., Rolston, D. E., 2007. Gas diffusivity and air permeability in a volcanic ash soil profile: Effects of organic matter and water retention. Soil Science 172 (6), 432–443.

Reynolds, R. C., 1971. Clay mineral formation in an alpine environment. Clays and Clay Minerals 19 (6), 361–374.

Rolston, D. E., Moldrup, P., 2002. 4.3 Gas Diffusivity. In: Dane, J. H., Topp, C. G. (Eds.), Methods of Soil Analysis: Part 4 Physical Methods. Vol. 4 of 5. Soil Science Society of America, Madison, WI, pp. 1113–1139.

Sakamoto, Y., Ishiguro, M., Kitagawa, G., 1986. Akaike Information Criterion Statistics. Vol. 1 of Mathematics and its Applications. Reidel Publishing Company, Dordrecht, The Netherlands.

Schjønning, P., 1985. A laboratory method for determination of gas diffusion in soil. Tech. Rep. S 1773, Beretning. Statens Planteavlsforsøg (Denmark), (in Danish with English summary).

Schjønning, P., Koppelgaard, M., 2017. The Forchheimer approach for soil air permeability measurement. Soil Science Society of America Journal 81 (5), 1045–1053.

Schjønning, P., Thomsen, I. K., Møberg, J. P., de Jonge, H., Kristensen, K., Christensen, B. T., 1999. Turnover of organic matter in differently textured soils: I. Physical characteristics of structurally disturbed and intact soils. Geoderma 89 (3), 177–198.

Schjønning, P., 1992. Size distribution of dispersed and aggregated particles and of soil pores in 12 Danish soils. Acta Agriculturae Scandinavica, Section B — Soil & Plant Science 42 (1), 26–33.

Schjønning, P., Eden, M., Moldrup, P., de Jonge, L. W., 2013. Two-chamber, two-gas and one-chamber, one-gas methods for measuring the soil-gas diffusion coefficient: Validation and inter-calibration. Soil Science Society of America Journal 77 (3), 729–740.

Schjønning, P., McBride, R. A., Keller, T., Obour, P. B., 2017. Predicting soil particle density from clay and soil organic matter contents. Geoderma 286, 83–87.

Schofield, R. K., 1935. The pF of the water in soil. In: Transactions of the Third International Congress of Soil Science. Vol. 2. International Society of Soil Science, Thomas Murby & Company, Oxford, pp. 37–48.

Six, J., Elliott, E. T., Paustian, K., Doran, J. W., 1998. Aggregation and soil organic matter accumulation in cultivated and native grassland soils. Soil Science Society of America Journal 62 (5), 1367–1377.

Smith, K., Watts, D., Way, T., Torbert, H., Prior, S., 2012. Impact of tillage and fertilizer application method on gas emissions in a corn cropping system. Pedosphere 22 (5), 604–615.

Soil Survey Staff, 1999. A basic system of soil classification for making and interpreting soil surveys. Agricultural Handbook 436, Natural Resources Conservation Service, USDA, Washington DC, USA.

Stepniewski, W., Stepniewska, Z., Rozej, A., Apr. 2011. 8 Gas Exchange in Soils. In: Hatfield, J. L., Sauer, T. J. (Eds.), Soil Management: Building a Stable Base for Agriculture. SSSA Book Series. Soil Science Society of America, Madison, WI, pp. 117–144.

Stine, R. A., 1985. Bootstrap prediction intervals for regression. Journal of the American Statistical Association 80 (392), 1026–1031.

Sugiura, N., 1978. Further analysts of the data by Akaike' s information criterion and the finite corrections. Communications in Statistics - Theory and Methods 7 (1), 13–26.

Taylor, S. A., 1950. Oxygen diffusion in porous media as a measure of soil aeration. Soil Science Society of America Journal 14 (C), 55–61.

Thorbjørn, A., Moldrup, P., Blendstrup, H., Komatsu, T., Rolston, D. E., 2008. A gas diffusivity model based on air-, solid-, and water-phase resistance in variably saturated soil. Vadose Zone Journal 7 (4), 1276–1286.

Uteau, D., Pagenkemper, S. K., Peth, S., Horn, R., 2013. Root and time dependent soil structure formation and its influence on gas transport in the subsoil. Soil and Tillage Research 132, 69–76.

Vereecken, H., Maes, J., Feyen, J., Darius, P., 1989. Estimating the soil moisture retention characteristic from texture, bulk density, and carbon content. Soil science 148 (6), 389–403.

Wagner, S., Cattle, S. R., Scholten, T., 2007. Soil-aggregate formation as influenced by clay content and organic-matter amendment. Journal of Plant Nutrition and Soil Science 170 (1), 173–180.

Weber, P. L., de Jonge, L. W., Greve, M. H., Norgaard, T., Moldrup, P., 2020. Gas diffusion characteristics of agricultural soils from South Greenland. Soil Science Society of America Journal 84 (5), 1606–1619.

Williamson, R. E., 1964. The effect of root aeration on plant growth. Soil Science Society of America Journal 28 (1), 86–90.

Yang, Z., Mohanty, B. P., Tong, X., Kuang, X., Li, L., 2021. Effects of water retention curves and permeability equations on the prediction of relative air permeability. Geophysical Research Letters, in press.

Yeasmin, S., Singh, B., Smernik, R. J., Johnston, C. T., 2020. Effect of land use on organic matter composition in density fractions of contrasting soils: A comparative study using 13C NMR and DRIFT spectroscopy. Science of The Total Environment 726, 138395.